A theoretical analysis for the effect of focal contact formation on cell-substrate attachment strength

Michael D. Ward and Daniel A. Hammer
School of Chemical Engineering, Cornell University, Ithaca, New York 14853 USA

ABSTRACT For many cell types, growth, differentiation, and motility are dependent on receptor-mediated adhesion to ligand-coated surfaces. Focal contacts are strong, specialized, adhesive connections between cell and substrate in which receptors aggregate and connect extracellular ligand to intracellular cytoskeletal molecules. In this paper, we present a mathematical model to examine how focal contact formation affects cellular adhesive strength.

To calculate adhesive strength with and without focal contacts, we use a one-dimensional tape peeling analysis to determine the critical tension necessary to peel the membrane. Receptor-ligand bonds are modeled as adhesive springs. In the absence of focal contacts, we derive analytic expressions for the critical tension at low and high ligand densities and show how membrane morphology affects adhesion. Then, focal contacts are modeled as cytoplasmic nucleation centers which bind adhesion receptors. The extent of adhesive strengthening upon focal contact formation depends on the elastic rigidity of the cytoskeletal connections, which determines the structural integrity of the focal contact itself. We consider two limits to this elasticity, very weak and rigid. Rigid cytoskeletal connections give much greater attachment strengths. The dependence of attachment strength on measurable model parameters is quite different in these two limits, which suggests focal contact structure might be deduced from properly performed adhesion experiments.

Finally, we compare our model to the adhesive strengthening response reported for glioma cell adhesion to fibronectin (Lotz et al., 1989. *J. Cell Biol.* 109:1795–1805). Our model successfully predicts the observed detachment forces at 4°C and yields values for the number of fibronectin receptors per glioma cell and the density of cytoskeletal connection molecules (talin) involved in receptor clusters which are consistent with measurements for other cell types. Comparison of the model with data at 37°C suggests that while cytoskeletal cross-linking and clustering of fibronectin receptors significantly increases adhesion strength, specific glioma cell-substratum attachment sites possess little mechanical rigidity and detach through a peeling mechanism, consistent with the view that these sites of $\leq$15 nm cell-substrate separation are precursors to fully formed, elastically rigid focal contacts.

INTRODUCTION

Receptor-mediated cell adhesion is an essential component of many biological responses including growth, differentiation, and motility. Firm attachment to a substrate is a prerequisite for the growth of certain cell types and several studies suggest the rate of cell growth is influenced by the extent of cell spreading (Ingber, 1990; O'Neill et al., 1986; Folkman and Moscona, 1978). For example, only highly adhesive surfaces which promote extensive spreading support the growth of endothelial cells (Ingber, 1990), consistent with the finding that nuclear events such as DNA synthesis are dependent on the area of contact between cell and substratum (O'Neill et al., 1986; Ben-Ze'ev et al., 1980). While cell growth requires strong cell-substrate attachment, cell differentiation is only observed as substrate adhesiveness is diminished (Watt et al., 1988; Ben-Ze'ev et al., 1988), suggesting that modulation of adhesive interactions may provide a potential biochemical control mechanism for differentiation (Ingber and Folkman, 1989). Finally, the formation of strong, specific attachment sites termed focal contacts is associated with reduced cell migration (Kolega et al., 1982; Izzard and Lochner, 1980; Couchman and Rees, 1979). Thus, a fundamental understanding of how cells regulate adhesive behavior should lead to improved knowledge of many aspects of cellular physiological behavior.

There are several potential mechanisms by which a cell may modulate adhesive behavior. According to the "stick and grip" hypothesis, adhesion is initially dependent on binding between cell surface adhesion receptors and substrate ligand molecules (Rees et al., 1977). Reinforcement and subsequent strengthening of this attachment may occur through: (*a*) an alteration of the structure of specific adhesive sites, driven by cytoskeletal events, which may change the strength of these sites; (*b*) a global accumulation of adhesion receptors in the area of contact or, more specifically, in localized regions within the adhesive contact; and (*c*) a realignment of the microfilament or microtubule networks which may alter cell mechanical properties and thus affect how bulk intracellular stresses are transmitted to the cell-substrate interface.

Significant progress has been made toward understanding both receptor-ligand binding events and the association of cytoskeletal elements with adhesion receptors. Within the integrin family of receptors are a number of molecules which mediate the attachment of cells to extracellular matrix molecules such as laminin, collagen, and fibronectin (Akiyama et al., 1990; Buck and Horwitz, 1987). In addition to binding extracellular ligands, experimental studies have demonstrated an inter-

Please address correspondence to Dr. Hammer

0006-3495/93/03/936/24 $2.00

action between the fibronectin receptor and the cytoskeletal molecule talin (Horwitz et al., 1986). Since talin can bind vinculin (Burridge and Mangeat, 1984), another cytoskeletal molecule which itself has a low affinity for α-actinin (Otto, 1990), a cross-linker of actin filaments, a linkage between the fibronectin receptor and the microfilament network could conceivably be mediated by a talin-vinculin-α-actinin chain (Burridge et al., 1988). This hypothesis is supported by immunofluorescent studies which have verified the colocalization of the fibronectin receptor, talin and vinculin at specific cell-substratum attachment sites (Dejana et al., 1988; Fath et al., 1989). Initially identified by interference reflection microscopy, these discrete attachment sites of <15 nm separation distance where receptor-ligand bonds cluster and associate with the ends of actin filaments have been termed focal contacts or focal adhesions (Izzard and Lochner, 1976). Studies of fibroblast and glioma cell adhesion to fibronectin-coated surfaces have shown that cross-linking and aggregation of cell-surface adhesion receptors by the cytoskeletal network substantially augments the adhesive strength above that obtained through receptor-ligand interactions alone (Lotz et al., 1989).

Many theoretical descriptions of the relationship between cell surface chemistry and adhesion have been developed to understand and quantify how receptor-ligand interactions affect cell attachment strength. Evans (1985*a, b*) examined the mechanical response of the cell membrane to stresses generated by the formation of specific adhesive cross-bridges when these cross-bridges were evenly or discretely distributed throughout the contact region. For a continuum of adhesive bonds, he found that the tension required to peel the membrane is equal to the tension induced by adhesion. Such is not the case for discrete attachments, where detachment tensions are significantly larger than those generated during attachment. Expanding on this theory by relating the kinetics of bond formation and breakage to the separation distance between receptor and ligand, Dembo and colleagues (1988) analyzed the time-dependent attachment and detachment of a cell to a surface. In this analysis, it was assumed adhesion receptors were immobile and unable to redistribute over the cell surface. More recent models of cell disaggregation examine the influence of receptor mobility on adhesive strength (Tözeren et al., 1989). However, in these latter studies, detailed calculations of the morphology of the cell-substrate interface were not performed.

Despite these works, the contribution of focal contact formation on attachment strength has not yet been addressed. In this paper, we present a detailed mathematical model of cell adhesion which investigates how receptor mobility, membrane mechanics, and cytoskeletal-receptor interactions affect the receptor-mediated attachment of cells to ligand-coated surfaces. In the absence of focal contacts, we extend the analyses of Evans (1985*a*) and Dembo et al. (1988) to include receptor redistribution and find that the attachment strength depends not only on the extent of binding within the adhesive contact, but also on the membrane morphology at the edge of contact. We then demonstrate how focal contacts, modeled as cytoplasmic adhesive plaques, induce the clustering of receptor-ligand bonds to very high densities. We show the magnitude of adhesive strength enhancement upon focal contact formation is dependent on the inherent mechanical rigidity of the focal contact. Finally, we apply these analyses to centrifugation experiments performed by Lotz and coworkers (1989) for glioma cell adhesion to fibronectin to explain their results quantitatively, verify our model, and distinguish between different detachment mechanisms for this cell type.

MATHEMATICAL MODEL

General adhesion model (no focal contacts)

The relevant geometry describing our system is shown in Fig. 1 *a*. Although the geometry of the cell-substratum adhesive interface is three dimensional, for computational simplicity we consider an axisymmetric cell. The position along the cell membrane is described by the arc-length, s, while the membrane location relative to the substratum is given by $x(s)$ and $y(s)$, where x is a measure of the horizontal position along the substrate and y represents the cell-substrate separation distance. There are two important membrane regions: (*a*) a macroscopic region over which adhesive interactions are negligible, and (*b*) a microscopic contact region, extending from the point $s = 0$ to the center of contact, defined by the membrane segment length, L, where the formation of receptor-ligand bonds supports attachment. A macroscopic tension, arising from any applied forces on the cell membrane, acts at an orientation determined by the macroscopic contact angle (θ_{mac}) and curvature.

Cell-substrate attachment is mediated by the specific interaction between membrane-bound adhesion receptors and extracellular ligand molecules located on a planar substrate. While ligand molecules are assumed to be fixed in position, the receptors can freely diffuse in the plane of the membrane. Previous theoretical models assumed immobile receptors, which imposed a limit on the maximum bond density (Dembo et al., 1988; Evans, 1985*a, b*). Although some receptors may be immobile, experimental studies have shown that many types of adhesion receptors can accumulate into localized clusters on the cell surface (Fath et al., 1989; Dejana et al., 1988; Duband et al., 1988). Since this redistribution may be an essential step in the adhesive strengthening response, we place no restrictions on receptor mobility.

At steady-state, we can write a balance between the

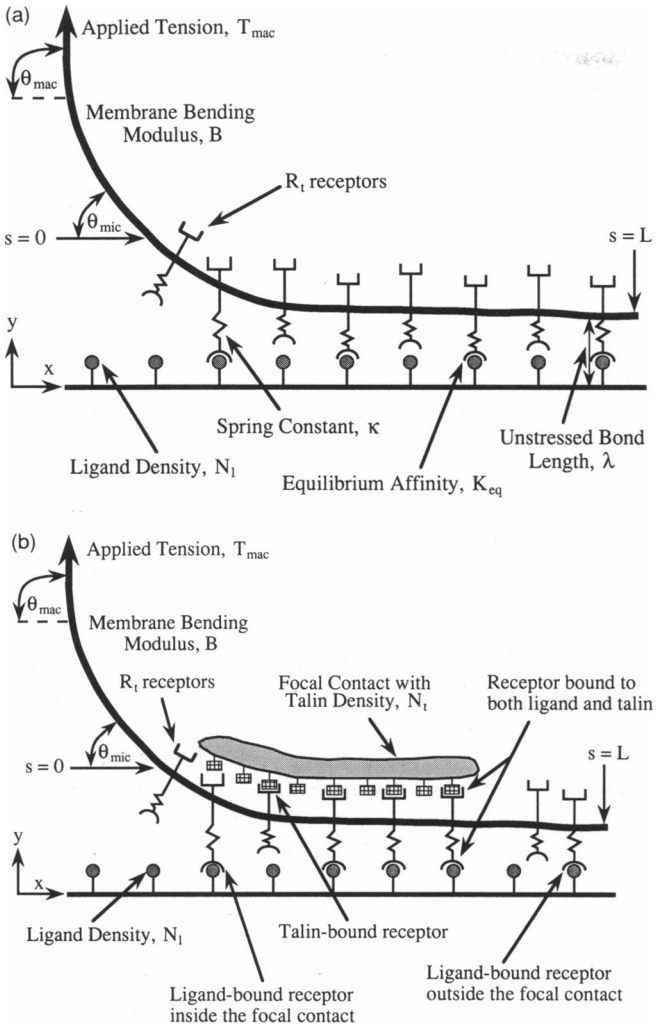

FIGURE 1 (*a*) We utilize a one-dimensional tape peeling analysis where the shape of a membrane segment of length L is given by $x(s)$ and $y(s)$. The point $s = 0$ divides the membrane into a macroscopic region, where an applied tension acts at a specified orientation, and a microscopic region, over which adhesion is mediated by specific receptor-ligand binding. Adhesion receptors are mobile in the plane of the membrane, while ligand molecules are fixed in location on the substrate. Receptor-ligand bonds are modeled as adhesive springs with a characteristic spring constant κ and unstressed length λ. (*b*) In the focal contact model, we introduce a cytoskeletal adhesive plaque containing talin molecules capable of interacting with the cytoplasmic portion of the adhesion receptors.

rate of formation of receptor-ligand bonds and the dissociation of these complexes:

$$0 = k_f(N_l - N_b)N_f - k_r N_b, \tag{1}$$

where N_l is the ligand density, N_b is the density of receptor-ligand bonds, N_f is the free receptor density, and k_f and k_r are the forward and reverse reaction rates. The finite number of adhesion receptors on the cell surface imposes a restriction on the maximum number of bonds which may form. This limit is represented by a material balance on the total number of receptors, R_t,

$$R_t = N_f A_{cell} + 2\pi \int_0^L N_b x \, ds. \tag{2}$$

where A_{cell} is the cell area.

Following the analysis of Dembo and co-workers (1988), we model the receptor-ligand bond as a Hookean spring with an unstressed length λ and spring constant κ. The affinity, K, is

$$K = \frac{k_f}{k_r} = K_{eq} \exp\left\{\frac{-\kappa(y-\lambda)^2}{2k_b\Theta}\right\}, \tag{3}$$

where K_{eq} is the affinity for an unstressed bond and $k_b\Theta$ is the thermal energy. Because the receptor-ligand affinity is diminished as bond strain increases, changes in membrane morphology will influence the extent of binding between cell and substrate.

We consider only steady state detachment and assume that the deformation of the model cell in the cell-substrate interface is governed by membrane mechanical properties. In this case, the morphology of the membrane in the microscopic contact region satisfies the equations of mechanical equilibrium for a thin, inextensible membrane (Dembo et al., 1988; Evans, 1985*a*, *b*):

$$B\frac{\partial^2 C}{\partial s^2} - CT = -\left[N_b\kappa(y-\lambda)\left(\frac{\partial x}{\partial s}\right)\right] \tag{4}$$

and

$$\frac{\partial T}{\partial s} + \left(\frac{B}{2}\right)\frac{\partial C^2}{\partial s} = \left[N_b\kappa(y-\lambda)\left(\frac{\partial y}{\partial s}\right)\right], \tag{5}$$

where T is the membrane tension, C is the membrane curvature, and B is the membrane bending modulus. These equations describe a balance between mechanical stresses, induced by membrane tensions and membrane bending, and chemical bonding stresses.

The arclength and curvature can be related to the Cartesian coordinate system:

$$\left(\frac{\partial x}{\partial s}\right)^2 + \left(\frac{\partial y}{\partial s}\right)^2 = 1, \tag{6}$$

and

$$C = \left(\frac{\partial x}{\partial s}\right)\left(\frac{\partial^2 y}{\partial s^2}\right) - \left(\frac{\partial y}{\partial s}\right)\left(\frac{\partial^2 x}{\partial s^2}\right). \tag{7}$$

Eqs. 1–7 completely describe the behavior of the cell membrane in the microscopic region subject to the appropriate boundary conditions and necessary matching equations between the microscopic and macroscopic regions (Appendix A).

Focal contact model

In addition to binding ligand molecules throughout the contact region, certain adhesion receptors can bind cytoskeletal molecules and form focal contacts. Because

these adhesive sites have been implicated in the strengthening of cell-substratum adhesion, we seek to develop a model which will provide insight into the causes of this strengthening. The geometry describing this extension of the model is shown in Fig. 1 *b*.

Several molecules which may provide a link between the fibronectin receptor of the integrin family and the actin microfilament network have been identified and include talin, vinculin, and α-actinin. Of particular interest is the molecule talin, which interacts directly with the fibronectin receptor (Horwitz et al., 1986) and associates with the precursor of the mature focal contact (DePasquale and Izzard, 1991). Although focal contacts form through a complex process involving extension, solidification, contraction, and dynamic restructuring of cytoskeletal elements, in this analysis we will treat the focal contact in a simple manner, since we are not interested in the dynamics or details of focal contact formation, but rather the strength of the resulting structure. Following the formation of the focal contact through active reorganization of the cytoskeleton, the focal contact must withstand any externally applied stresses caused during the detachment phase of an adhesion assay in addition to actively generated contractile stresses. Although contractile stresses might be significant over local regions of the cell-substrate interface, we assume that active cytoskeletal forces are, overall, small compared to externally applied detachment forces, such that the contribution of focal contacts can be modeled as the passive response of the focal contact to applied stresses. (In the General Results section, we show that the passive response of these dynamically assembled structures is sufficiently strong to account for orders of magnitude increases in adhesion strength without employing any specific, active resistance to detachment on the part of these structures.) We model the fully mature focal contact as a cytoskeletal plaque containing molecules, which we shall generically call talin, capable of binding the cytoplasmic portion of the adhesion receptors. These molecules are presumed to have the same binding characteristics as talin and to be evenly distributed throughout the focal contact. Since examination of published immunofluorescent micrographs indicates that the majority of focal contacts are associated near the cell periphery (Wayner et al., 1991; Fath et al., 1989; Burridge and Connell, 1983), we place the cytoplasmic adhesive plaque at the edge of the microscopic contact region.

For membrane locations outside the focal contact, a modified version of Eq. 1 gives the mass balance between bound and free receptors,

$$0 = k_f(N_l - N_{bo})N_f - k_r N_{bo}, \quad (8)$$

where N_{bo} is the density of receptor-ligand bonds outside the focal contact.

Within the focal contact, three bound species may be present: receptors bound to ligand only, receptors bound to talin only, and receptors bound to both ligand and talin. The respective material balances for each of these complexes are:

$$0 = k_f(N_l - N_{bi} - N_{bc})N_f - k_r N_{bi} + k_r^t N_{bc} - k_f^t(N_t - N_c - N_{bc})N_{bi}, \quad (9)$$

$$0 = k_f^t(N_t - N_c - N_{bc})N_f - k_r^t N_c + k_r N_{bc} - k_f(N_l - N_{bi} - N_{bc})N_c \quad (10)$$

and

$$0 = k_f(N_l - N_{bi} - N_{bc})N_c + k_f^t(N_t - N_c - N_{bc})N_{bi} - k_r N_{bc} - k_r^t N_{bc}, \quad (11)$$

where N_t is the talin density, N_{bi} is the density of receptor-ligand bonds within the focal contact, N_c is the density of receptor-talin bonds, N_{bc} is the density of doubly-bound receptors, and k_f^t and k_r^t are the forward and reverse rates for receptor-talin binding. Receptor and talin molecules are assumed to interact with constant affinity K_{eq}^t ($=k_f^t/k_r^t$), whereas receptor-ligand bonds are modeled as adhesive springs and will therefore be affected by membrane morphology.

The bond densities inside and outside the focal contacts are linked through conservation of receptors,

$$R_t = N_f A_{cell} + (N_{bo})(\pi L^2 - N_{fc}A_{fc}) + (N_{bi} + N_c + N_{bc})(N_{fc}A_{fc}), \quad (12)$$

where A_{fc} is the area of each focal contact and N_{fc} is the total number of focal contacts.

For purposes of estimating the free receptor density only, we assume the contact area is flat at a separation distance equal to the unstressed length of a receptor-ligand bond (Appendix B). This approximation is acceptable since the maximum boundary length over which bonds are stretched (Evans, 1985*a*) is much less than the typical contact radius of a spread cell. Eqs. 8–12 completely describe the binding within the adhesive region; once an estimate of N_f is obtained, N_{bo}, N_{bi}, N_c, and N_{bc} are calculated exactly as functions of separation distance.

The formation of adhesive bonds will produce stresses on the membrane which must be balanced by membrane tensions and bending. We assume all receptor-ligand bonds, including those also bound to the cytoskeleton, contribute to membrane stresses. In this case, N_b is replaced by either N_{bo} or $N_{bi} + N_{bc}$ in Eqs. 4 and 5, depending on whether we are outside or inside the focal contact, respectively.

MODES OF DETACHMENT

General adhesion model (no focal contacts)

The detachment of a cell from a substrate can be likened to the peeling of an adhesive material in which macro-

scopic tensions above the critical tension, T_{crit}, initiate peeling (Dembo et al., 1988; Evans, 1985*a, b*). We are interested in determining the applied force necessary to initiate detachment, which to a first approximation can be related to the critical tension using a force balance,

$$F_d \approx 2\pi L T_{crit}. \tag{13}$$

Dembo and co-workers (1988) previously derived an analytic expression for the critical tension in the case of immobile adhesion receptors. In this analysis, the adhesive energy density was proportional to the total receptor density. However, for mobile receptors we expect a different functionality. When the ligand density (N_l) is small, relatively few adhesion receptors will be bound and we can approximate the free receptor density as R_t/A_{cell}. Following the procedure of Dembo et al. (1988), we write the bond density as a power series in the peeling velocity, where the coefficients of this series are obtained through algebraic manipulation of Eq. 1. Substituting this series into the tangential force balance and integrating from $s = -\infty$ to $s = L$, we obtain the following expression for the critical tension in the limit of low ligand density,

$$T_{crit} = \frac{N_l k_b \Theta \ln\left(1 + \frac{R_t K_{eq}}{A_{cell}}\right)}{1 - \cos\theta_{mac}}. \tag{14}$$

When N_l is high, all receptors will be bound and the bond density can be approximated as $R_t/\pi L^2$. Because these cross-bridges are evenly and continuously distributed in the adhesive contact, the work required to detach the membrane is equal to the adhesive energy, χ, and can be related to the macroscopic tension ($=T_{crit}$) by Young's equation (Evans, 1985*a*),

$$\chi = T_{crit}(1 - \cos\theta_{mac}). \tag{15}$$

For a cell bound to a substrate through spring-like bonds, the work required to bring a flat membrane from a separation distance of λ to a length l_b is $\chi = N_b\kappa(l_b - \lambda)^2/2$, where l_b is the length the bond may extend before rupture. Additionally, if the deformation of the receptor-ligand bond occurs through stretching of α-helical or random coil protein segments, the spring constant can be approximated by $k_b\Theta/l_h^2$, *where* l_h is the length of an α-helical segment (Bell et al., 1984). Substituting these expressions into Eq. 15 yields:

$$T_{crit} \approx \frac{R_t k_b \Theta}{\pi L^2(1 - \cos\theta_{mac})}\left(\frac{(l_b - \lambda)^2}{2l_h^2}\right). \tag{16}$$

The forces required to rupture an adhesive bond or extract a receptor from the lipid bilayer have either been measured or estimated and are in the vicinity of 1 μdyn (Evans et al., 1991; Tha and Goldsmith, 1988; Bell, 1978). For an adhesive spring, comparable forces are obtained for values of l_b and l_h such that $(l_b - \lambda)^2/2l_h^2 \sim$ 3 to 5. However, this derivation assumes the separation of an adhesive contact in which all bonds are initially unstressed. Since some bonds at the edge of contact will be initially stretched during peeling, Eq. 16 will slightly overestimate the true critical tension and we can approximate T_{crit} in the limit of high ligand density as:

$$T_{crit} \approx \frac{R_t k_b \Theta}{\pi L^2(1 - \cos\theta_{mac})}. \tag{17}$$

Therefore, the critical tension for mobile receptors in the limits of low and high N_l will be given by Eqs. 14 and 17, respectively. Note the critical tension for mobile receptors is proportional to ligand density for high receptor numbers (R_t) or low N_l (14) and to receptor number for low R_t or high N_l (17). Finally, the exact value for T_{crit} may be obtained over the full range of ligand densities through numerical integration of the tangential force balance (Eq. 5) from the macroscopic region to the center of the adhesive contact.

Focal contact model

In addition to enhanced binding within the focal contact, the inherent mechanical elasticity of the cytoskeletal plaque may have a profound effect on the forces required to break the contact and initiate cell detachment. In this analysis, we will consider two possible limiting cases (Fig. 2): (*a*) the cytoskeletal elements of the focal contact add no additional mechanical stiffness to the membrane such that the stiffness of the focal contact-membrane structure is the same as that of the membrane itself, and (*b*) the cytoskeletal components of the focal contact are totally rigid. Through comparison of our model to experimental data on cell detachment, we hope to determine which limit of focal contact elasticity more closely resembles the true response of the focal adhesion to an applied force.

When the focal contact adds no additional stiffness, detachment of the focal contact occurs through a progressive breaking of bonds at the cell periphery. Any enhancement in adhesive strength arises solely from increased clustering of bonds within the focal adhesion. This limit gives the minimum possible adhesive strengthening that can occur with focal contact formation. To calculate the force to peel a focal contact-bound cell, we assume that stresses are applied evenly around the cell periphery. Because of enhanced receptor clustering within the focal contact, cell-substrate adhesion is much stronger at these sites than at other regions of the cell surface. Hence, the limiting resistance of the cell to a macroscopic applied force can be related to a mechanical tension acting solely on the focal contacts. Provided the majority of focal contacts are located at the cell periphery and that all contacts are identical, the detachment force will simply equal the force required to peel all focal contacts at the cell margin. (In the Model Analysis section, we cite evidence for the peripheral distribution of focal adhesions in the cell-sub-

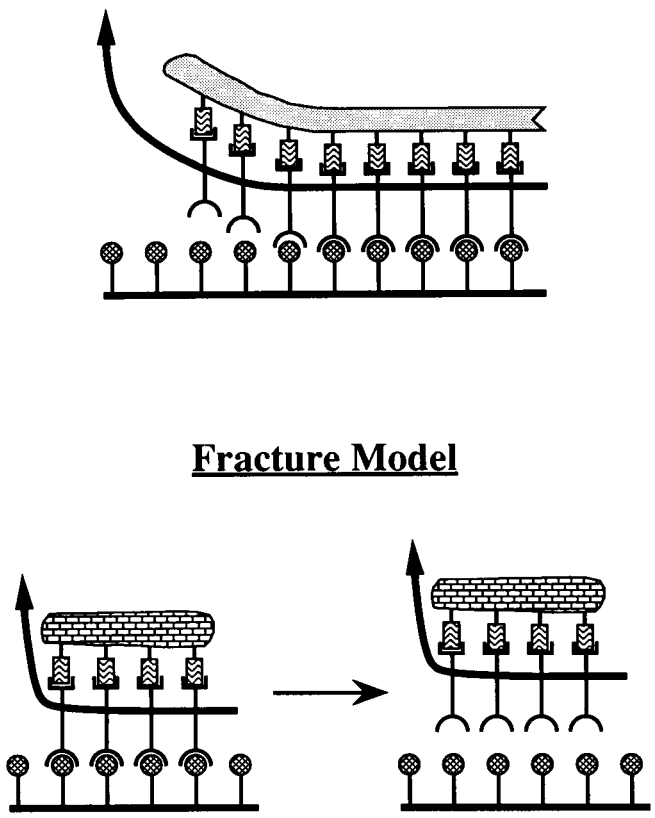

FIGURE 2 Detachment of our model focal contact-containing cell occurs through one of two distinct mechanisms: peeling or fracture. In the peeling model, the focal contact has no mechanical rigidity and thus detachment proceeds through progressive bond breakage at the edge of contact. This mechanism represents the minimum detachment force. Because the focal contact is a totally rigid entity in the fracture model, detachment requires distribution of stress equally among all receptor-ligand bonds within the focal contact. Since all receptor-ligand bonds within the focal contact participate in establishing focal adhesion strength, fracture gives the maximum detachment force.

strate interface obtained from our detailed analysis of published immunofluorescent micrographs.) The detachment force can then be related to the critical tension to peel an individual focal contact:

$$F_{d,\text{peel}} = (0.7N_{fc}W_{fc})T_{\text{crit}}, \tag{18}$$

where $F_{d,\text{peel}}$ is the force to detach the cell through peeling of focal contacts, W_{fc} is the width of the focal contact, and we have assumed 70% of the focal contacts are near the contact periphery. To determine the critical tension for peeling a focal contact, the tangential force balance must be numerically integrated over the length of the focal adhesion.

In the second model of the focal contact, we treat the contact as a totally rigid structure in which applied stresses are equally distributed to all the receptors in the focal contact simultaneously. Detachment is initiated when a single bond breaks, leading to fracture of the remaining cross-bridges. This limit represents the maximum adhesive strength because the entire focal contact shares the applied load. The force to detach a cell by fracture, $F_{d,\text{fracture}}$, is:

$$F_{d,\text{fracture}} = (0.7N_{fc}A_{fc})(N_{bi} + N_{bc})F_{\text{bond}}, \tag{19}$$

where F_{bond} is the force to rupture a single receptor-ligand bond. We will assume that $F_{\text{bond}} = 1$ μdyn, consistent with theoretical estimates for the bond strength (Bell, 1978), and measurements of the force required to separate agglutinated red blood cells (Tha and Goldsmith, 1988) or uproot individual glycophorin molecules from the red blood cell membrane (Evans et al., 1991).

Following cell detachment, pieces of cell membrane are often observed to remain adherent to the substrate because of membrane rupture (Weiss and Lachmann, 1964; Weiss, 1961). Applied membrane tensions required to lyse lipid bilayers and red blood cells are in the range 1–15 dyn cm^{-1} (Evans and Needham, 1986; Evans et al., 1976). We can compare the tensions generated by peeling or fracture of the focal contact to lysis tensions to determine if membrane rupture is possible in either case. For the peeling model, the maximum membrane tension will equal the critical tension. The membrane tension is not explicitly determined in the fracture model; however we can estimate the tension if we assume that the detachment force is proportional to the tension at the focal contact edge and the length over which this tension is applied. To make this estimate, we assume the focal contact is rectangular in shape and the applied force is equally distributed around the perimeter of the focal contact. The membrane tension generated during fracture is then:

$$T \approx \frac{F_{d,\text{fracture}}}{(0.7N_{fc})(2L_{fc} + 2W_{fc})}, \tag{20}$$

where L_{fc} is the length of the focal contact.

MODEL ANALYSIS

Table 1 lists estimates of the dimensional parameters involved in this analysis. We have drawn a distinction between general parameters which may be suitable for all cell types, and those which apply specifically to the glioma cell adhesion studies of Lotz and colleagues (1989), which we shall analyze later in this paper. Although many of these parameter estimates have been determined from experimental studies, the number of focal contacts found per cell, the location of these contacts, and the density of talin molecules within the focal contact are parameters which to our knowledge have not been unambiguously reported in any system.

In order to estimate the number of focal contacts per cell, we analyzed published immunofluorescent micro-

TABLE 1 **Estimates for dimensional parameters of the model**

Parameter	Definition	Physiological range	"Best" value	Glioma-FN value	Source
A_{cell}	Cell area	10^2–10^4 μm^2	1,000 μm^2	2,000 μm^2 *	Bell et al., 1984
A_{fc}	Focal contact area	0.5–5.0 μm^2	1.0 μm^2	1.0 μm^2 *	Izzard and Lochner, 1976
B	Bending modulus	0.4–4.0 $\times 10^{-12}$ ergs	10^{-12} ergs	10^{-12} ergs	Duwe et al., 1990 Engelhardt et al., 1985 Evans, 1983
$k_b\Theta$	Thermal energy	3.8–4.3 $\times 10^{-14}$ ergs	4.1 $\times 10^{-14}$ ergs	3.8–4.3 $\times 10^{-14}$ ergs	—
k_r, k_r^t	Reverse reaction rates	10^{-5}–$10^1 s^{-1}$	10^{-1} s^{-1}	$10^{-1} s^{-1}$	Bell, 1978 Pecht and Lancet, 1977
K_{eq}	Receptor-ligand equilibrium affinity	10^{-10}–10^{-5} cm^2	10^{-8} cm^2	5.0 $\times 10^{-9}$ cm^2	Bell et al., 1984
K_{eq}^t	Receptor-talin equilibrium affinity	10^{-9}–10^{-6} cm^2	$10^{-8}cm^2$	5.0 $\times 10^{-9}$ cm^2	Horwitz et al., 1986 Otey et al., 1990
L	Contact radius	5–30 μm	10 μm	8.08–15.7 μm	Bell et al., 1984
N_{fc}	Number of focal contacts	0–>120	0–157	0–172*	Estimated‡ from Burridge and Connell, 1983 Fath et al., 1989 Nuckolls et al., 1990 Wayner et al., 1991
	Location of focal contacts	Mostly at periphery	70% at periphery	70% at periphery*	Estimated‡ from Burridge and Connell, 1983 Fath et al., 1989
N_l	Ligand density	10^6–10^{12} cm^{-2}	10^{11} cm^{-2}	$10^{12}cm^{-2}$ *	Danilov and Juliano, 1989 Jones et al., 1986 Massia and Hubbell, 1991
N_t	Talin density	10^9–10^{12} cm^{-2}	10^{11} cm^{-2}	1.5–5.0 $\times 10^{11}$ cm^{-2} *	Estimated‡ from Feltkamp et al., 1991
R_t	Number of receptors	10^4–10^6	10^5	1.4–3.4 $\times 10^5$ *	Bell et al., 1984
λ	Unstressed receptor-ligand bond length	10–100 nm	15 nm	15 nm	Bell et al., 1984
κ	Spring constant	10^{-2}–10^1 dyn cm^{-1}	1.0 dyn cm^{-1}	1.0 dyn cm^{-1}	Bell et al., 1984 Dembo et al., 1988

* These parameters were either estimated or deduced from comparison of theory to experiment. A description of this analysis can be found in the Comparison with Experiment section of the text.

‡ The detailed arguments for deriving these estimates are presented in the Model Analysis section of the text.

graphs of a number of different cell types and computed the number of focal contacts in the adhesive region. Cells initially in contact with a substrate contain relatively few focal adhesions, if any, while spread cells can easily have more than 100 focal contacts which account for roughly 5–15% of the total adhesive contact area (Wayner et al., 1991; Nuckolls et al., 1990; Fath et al., 1989; Burridge and Connell, 1983). We estimate that approximately 70% of the focal adhesions are located in the peripheral regions of the cell-substrate interface (Fath et al., 1989; Burridge and Connell, 1983), consistent with the finding that the strongest adhesive contacts between cell and substrate are predominantly confined to the cell margins (Harris, 1973). Since we have examined several different cell-substrate systems, we feel that these ranges are quite reasonable to describe generic cells forming focal adhesions with a surface.

Feltkamp and colleagues (1991) examined the distribution of talin and vinculin in focal adhesions of chicken embryo fibroblasts using a 'wet-cleaving' technique followed by immunoelectron microscopy. Analyzing their published micrographs, and assuming that only one gold-conjugated particle bound to each talin molecule, we estimate a talin density of $1.75 \pm 0.68 \times 10^{11}$ cm^{-2}. Since it is quite possible more than one gold particle was bound to each talin molecule, or that some talin molecules were inaccessible to the labelled antibodies or removed during fixation, this density is only an approximation to the true talin density.

Based on the results of experimental studies of the distribution of adhesion receptors on adherent cells, which indicate that virtually all of the receptors are associated with focal contacts (Fath et al., 1989; Duband et al., 1988; Dejana et al., 1988), we can estimate a lower bound on the talin density. Assuming that a well spread cell has a minimum of 10^4 adhesion receptors, an adhesive contact area equal to 2,000 μm^2 of which 10% is occupied by focal contacts, and that every talin molecule is bound to a receptor, a talin density of 5×10^9 cm^{-2} is necessary to bind every receptor. This calculation suggests the minimum possible talin density will be $\approx 10^9$ cm^{-2}.

Talin is a highly elongated, flexible molecule with a length of nearly 60 nm (Molony et al., 1987). To determine the maximum talin density, we consider the close packing of a talin molecule 60 nm in length and 5 nm in diameter. Depending on whether talin is projected length-wise or end-wise onto the two-dimensional cyto-

TABLE 2 **Dimensionless parameters**

Symbol	Expression	Definition
α	$\frac{2\pi L^2}{A_{cell}}$	Dimensionless contact area
α_{fc}	$\frac{N_{fc}A_{fc}}{A_{cell}}$	Dimensionless focal contact area
β	$\frac{\kappa\lambda^2}{2k_b\Theta}$	Bond energy/thermal energy
γ_{fc}	$\frac{N_t}{N_l}$	Talin density/ligand density
δ	$\frac{\lambda}{L}$	Bond length/contact area radius
ϵ	$\frac{A_{cell}N_l}{R_t}$	Ligand density/receptor density
ϕ	$\frac{\kappa L^2}{B}$	Bond energy/bending energy
ζ	$\frac{R_t L^2}{A_{cell}}$	Dimensionless receptor density
ω	$\frac{R_t K_{eq}}{A_{cell}}$	Dimensionless receptor-ligand affinity
ω_{fc}	$\frac{R_t K'_{eq}}{A_{cell}}$	Dimensionless receptor-talin affinity
ψ_{fc}	$\frac{k'_r}{k_r}$	Ratio of reverse reaction rates

skeletal plaque, N_t will be in the range 0.3–4 $\times$ 10^{12} cm^{-2}. We thus estimate the maximal N_t to be $\approx 10^{12}$ cm^{-2}.

The relevant scalings and non-dimensional equations are described in Appendix A. Table 2 lists the dimensionless groups which govern the behavior of the model. In the absence of focal contacts, we expect the attachment strength will depend on the total number of ligand molecules available for binding, $\epsilon\zeta$, and the dimensionless receptor-ligand affinity, ω.

Several additional dimensionless groups are required when focal contacts are present. Changes in the dimensionless receptor-talin affinity, ω_{fc}, and talin density, γ_{fc}, may affect the extent of binding within the focal contact. Increases in the number of focal contacts is accomplished through changes in either α_{fc}, which is the dimensionless focal contact area, or $2\alpha_{fc}/\alpha$, which measures the percentage of the adhesive contact area occupied by focal contacts.

GENERAL RESULTS

General adhesion model (no focal contacts)

Fig. 3 *a* shows the dependence of the critical tension on $\epsilon\zeta$, the number of ligand molecules available within the entire contact region, and the total number of adhesive receptors, R_t. For low $\epsilon\zeta$, T_{crit} increases linearly with ligand density but only logarithmically on receptor number, consistent with Eq. 14. When $\epsilon\zeta$ is much larger than R_t, T_{crit} is independent of ligand density but proportional to R_t, and the critical tension approaches the limit predicted by Eq. 17. Between the asymptotic limits at low and high ligand densities there is an intermediate $\epsilon\zeta$ at which T_{crit} is a maximum. Beyond this point, further increases in ligand density reduce the adhesive strength. This decrease can not be attributed to diminished receptor-ligand binding in the adhesive contact (Fig. 3 *b*), since bond formation increases with ligand density until all receptors are bound.

To understand this maximum in T_{crit}, consider that the tension necessary to initiate peeling will be affected

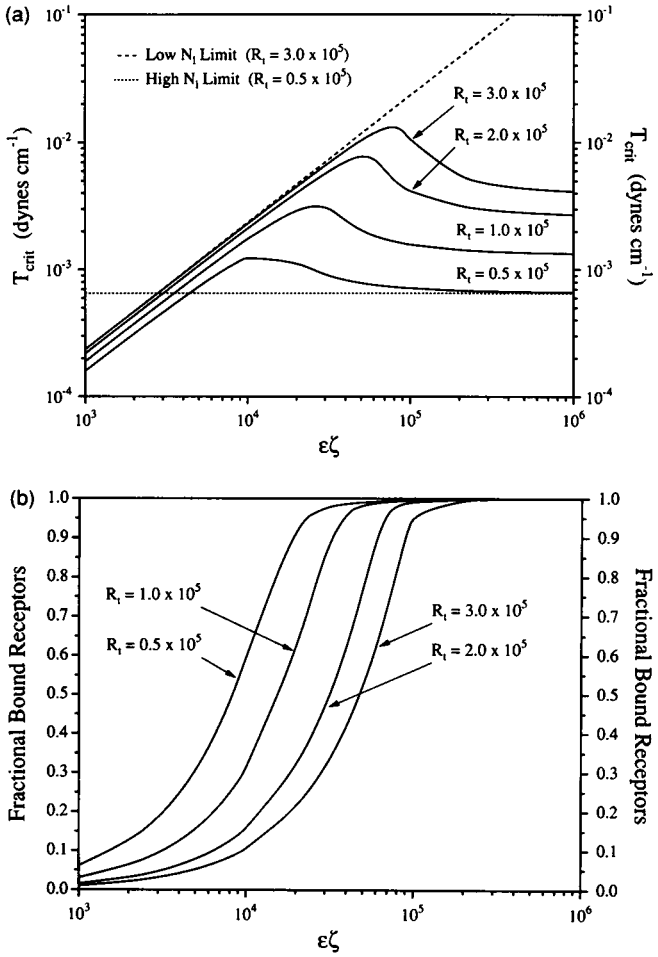

FIGURE 3 We plot the critical tension and the fraction of bound receptors as a function of the dimensionless ligand density, $\epsilon\zeta$, for different values of the receptor number, R_t. (*a*) The dependence of T_{crit} on $\epsilon\zeta$ and R_t at low and high ligand densities is consistent with the analytic expressions for T_{crit} (Eqs. 14 and 17). In addition, T_{crit} exhibits a maximum at an optimum ligand density. (*b*) The decrease in T_{crit} at high $\epsilon\zeta$ can not be attributed to reduced binding, as we show that the fraction of bound receptors increases as $\epsilon\zeta$ is increased. Parameter values for this simulation are $\alpha = 0.628$, $\beta = 27.4$, $\delta = 1.5 \times 10^{-3}$, $\phi = 10^6$, and $\omega/\zeta = 0.01$. $C_{mac} = 0$ cm^{-1} and $\theta_{mac} = 90°$ for this and all subsequent simulations.

by the membrane morphology and bond density at the edge of contact, and hence depends on the microscopic contact angle. As shown in Fig. 4, a maximum in θ_{mic} as a function of ligand density results from a balance between the adhesive and bending energies at the edge of contact: increased adhesive energies will support greater membrane bending. At low $\epsilon\zeta$, since virtually all ligand molecules within the contact region will be bound, increases in ligand density give rise to enhanced binding throughout the entire contact region, including at the contact periphery, and therefore lead to larger θ_{mic} and T_{crit}. However, when $\epsilon\zeta$ is large, there is a substantial recruitment of receptors from the contact periphery to the contact interior where bonds are unstressed. Increasing $\epsilon\zeta$ in this regime will diminish the adhesive energy at the edge of contact, and thus result in decreased θ_{mic} and T_{crit}. This section illustrates that it is critical to account for membrane morphology for a rigorous determination of adhesive strength, even in the absence of focal attachments.

An additional prediction can be made about the role of receptor-ligand affinity in modulating the adhesion strength in the absence of focal contact formation. According to Eqs. 14 and 17 and Fig. 5, the critical tension should be logarithmically dependent on the receptor-ligand affinity (ω) at low ligand densities ($\epsilon\zeta$) and independent of the affinity at high ligand densities.

Although one might expect membrane rigidity to influence the critical tension, we find that changes in the bending modulus, B, affect membrane morphology but do not alter the adhesive strength (results not shown). This finding is consistent with theoretical studies on the kinetics of cell detachment which indicate that the rate of peeling, but not the tension necessary to initiate peeling, is affected by membrane rigidity (Dembo et al., 1988).

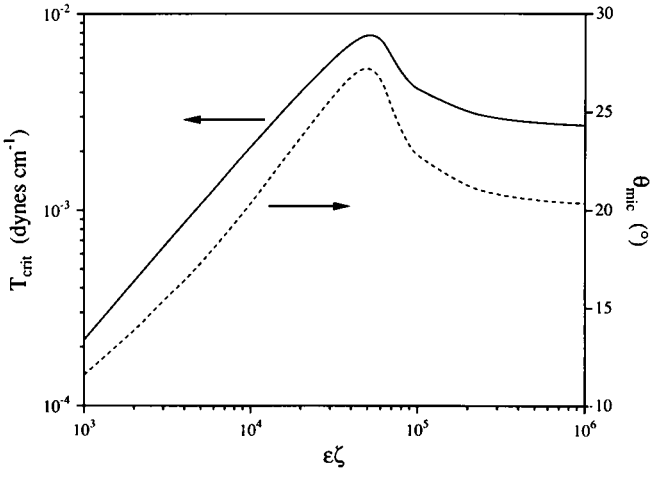

FIGURE 4 The dependence of the critical tension (*solid line*) and microscopic contact angle (*dashed line*) on the dimensionless ligand density, $\epsilon\zeta$. The reduction in T_{crit} at high $\epsilon\zeta$ coincides with diminished microscopic contact angles, suggesting that the adhesive strength is dependent on membrane morphology at the edge of contact. Parameter values are identical to those given in Fig. 3 and $\omega = 200$.

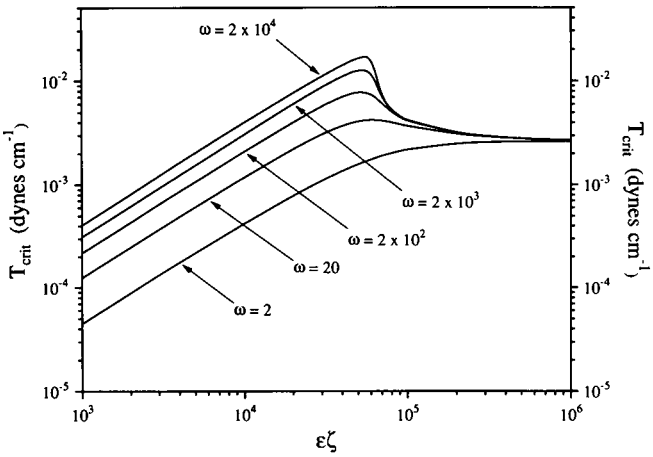

FIGURE 5 A plot of the critical tension versus the dimensionless ligand density, $\epsilon\zeta$, for different values of the dimensionless receptor-ligand affinity, ω. Consistent with the analytic expressions for T_{crit} derived in the text, T_{crit} is weakly dependent on affinity at low ligand densities and independent of ω at large $\epsilon\zeta$. Parameter values are given in Fig. 3 with $\zeta = 2 \times 10^4$.

Focal contact model

We next examine the effect of focal contact formation on adhesive strength. For these general simulations, we define a dimensionless detachment force, $\bar{F}_d$, and dimensionless critical tension, $\bar{T}_{crit}$,

$$\bar{F}_d = \frac{F_{d,fc}}{F_{d,\text{no } fc}}$$

and

$$\bar{T}_{crit} = \frac{T_{crit,fc}}{T_{crit,\text{no } fc}},$$

where $F_{d,fc}$ ($T_{crit,fc}$) is the force (critical tension) necessary to detach a focal contact-containing cell through either peeling or fracture, and $F_{d,\text{no } fc}$($T_{crit,\text{no } fc}$) is the detachment force (critical tension) to remove an identically endowed cell which lacks focal contacts through membrane peeling. These dimensionless quantities reflect the enhancement of the adhesive strength or critical tension due to the formation of focal adhesions. We also examine how the presence of cytoskeletal plaques affects the extent of receptor clustering, which is measured by the dimensionless bond density, $\bar{N}_{b,fc}$,

$$\bar{N}_{b,fc} = \frac{(N_{bi} + N_{bc})}{N_{b,\text{no } fc}},$$

where N_{bi} and N_{bc} are the density of ligand-bound and doubly-bound receptors within the focal contact, respectively, and $N_{b,\text{no } fc}$ is the bond density for a cell without focal contacts.

Receptor clustering occurs when the receptor-ligand bond density within the focal adhesion exceeds the bond density over the rest of the contact area. When receptors outnumber available ligand molecules (e.g., at low N_l), virtually all ligand molecules within the adhesive contact region are bound, resulting in a constant bond density over the entire contact region, thereby preventing clustering. In contrast, at high ligand densities, there is sufficient ligand to support redistribution and accumulation of receptors into focal contacts. Therefore, receptor aggregation within focal contacts will be greatest at high ligand densities.

These expectations are supported by the model results shown in Fig. 6 *a*, where the dimensionless bond density, $\bar{N}_{b,fc}$, is plotted as a function of the total number of talin molecules ($N_t N_{fc} A_{fc}$) and ligand molecules ($\epsilon\zeta$) available for binding. Below a minimum ligand density, there is negligible clustering ($\bar{N}_{b,fc} = 1$) even at high talin densities. As $\epsilon\zeta$ increases, receptor accumulation into focal contacts becomes substantial, with the greatest extent of clustering occurring at high N_t. Consider cases when $\epsilon\zeta \geq 10^5$. When N_t is low, the density of talin molecules limits the amount of receptor clustering, such that increases in N_t enhance the aggregation of receptors within focal contacts. When talin molecules are present in large excess, a maximum $\bar{N}_{b,fc}$ is reached where either the ligand density or number of receptors controls the extent of clustering. For example, in the high N_t regime, when $\epsilon\zeta < 10^6$, the bond density within the focal contact is restricted by the available ligand; increasing $\epsilon\zeta$ will enhance $\bar{N}_{b,fc}$. In contrast, when $\epsilon\zeta = 10^6$, the number of receptors limits the amount of clustering so that further increases in ligand density have no effect on $\bar{N}_{b,fc}$.

The associated dimensionless force to peel a cell with focal contacts is shown in Fig. 6 *b*. There is not a strict correlation between the number of receptors in a focal contact and cell adhesion strength when focal contacts peel. When clustering is negligible (low $\epsilon\zeta$ or $N_t N_{fc} A_{fc}$), the detachment force for cells with and without focal contacts are identical ($\bar{F}_d = 1$). Increases in adhesive strength observed at intermediate values of $\epsilon\zeta$ ($\leq 2 \times 10^5$) closely correspond to the enhanced clustering observed in Fig. 6 *a*, except at high talin densities where $\bar{N}_{b,fc}$ is constant but $\bar{F}_d$ continues to rise. At these talin densities, the distribution of bonds throughout the focal contact becomes more uniform, increasing the adhesion energy at the contact edge without significantly changing the total number of bonds within the focal contact. When $\epsilon\zeta$ is high, increases in N_t actually decrease the adhesion strength, although $\bar{N}_{b,fc}$ remains constant. This reduction in $\bar{F}_d$ at high N_t is a result of the redistribution of bonds from the edge to the interior of the focal contact. Finally, for these calculations the increase in adhesive strength upon focal contact formation can be as high as six-fold ($\bar{F}_d = 6$) if the focal contact peels during detachment.

In contrast, there is a strict correlation between receptor clustering in focal contacts and adhesion strength if the focal contacts fracture (Fig. 6 *c*). Most importantly, while the peeling model predicts a maximum six-fold increase in $\bar{F}_d$, fracture may require forces almost 10,000 times larger than those necessary to detach a cell which lacks focal contacts. This tremendous enhancement of the adhesive strength is primarily the result of the increased elastic rigidity of the focal contact since even a small degree of receptor clustering (low $\epsilon\zeta$ or $N_t N_{fc} A_{fc}$) leads to a several hundredfold increase in $\bar{F}_d$.

While it is well established that a cell can modulate attachment strength through upregulation of receptors or increased secretion of adhesive ligands, little is known concerning the effects of altered talin expression or receptor-talin affinity on adhesion. However, interactions between adhesion receptors and cytoskeletal molecules could be regulated intracellularly, and would therefore provide an attractive method for rapid and efficient cellular control of adhesive strength. In order to investigate this possibility, we examine the influence of receptor-talin avidity and talin density on adhesive strength (Fig. 7).

Fig. 7 *a* illustrates the dependence of the dimensionless critical tension necessary to peel the focal contact, $\bar{T}_{crit}$, as a function of the dimensionless receptor-talin affinity, ω_{fc}, and talin density, γ_{fc}. $\bar{T}_{crit}$ increases with increasing ω_{fc}. At low affinities, $\bar{T}_{crit}$ also increases with the talin density. However, at high affinities, there is a maximum in $\bar{T}_{crit}$ as a function of γ_{fc}, with the small decrease in $\bar{T}_{crit}$ at high talin densities once again due to redistribution of receptors away from the edge of contact. In these simulations, the tension required to initiate peeling can be 40-fold greater than the tension to peel a similar cell which lacks focal contacts.

Fig. 7 *b* shows the corresponding plot of dimensionless peeling force versus receptor-talin affinity and talin density. Since the peeling force is proportional to the critical tension, the curves in Fig. 7 *b* exhibit the same qualitative features as those in Fig. 7 *a*. Although there is no significant strengthening of adhesion at low ω_{fc} or γ_{fc}, increasing either the receptor-talin affinity or talin density can enhance the attachment strength by almost an order of magnitude. (Because the critical tension is presumed to act only on peripheral focal contacts in the peeling model (Eq. 18) and not along the entire periphery as in the absence of focal contacts (Eq. 13), $\bar{F}_d$ is always less than $\bar{T}_{crit}$.) In Fig. 7 *c*, we present similar results for the effect of receptor-talin affinity and talin density on the dimensionless fracture force, which indicate that fracture requires 1,000-fold greater forces than peeling. Interestingly, one difference between focal contact fracture and peeling appears to be that changes in the receptor-talin affinity have only a modest influence on the adhesion strength in fracture, but may substantially affect the adhesive strength in peeling (for example, compare curves in Fig. 7, *b* and *c*, labeled $\gamma_{fc} = 1.0$).

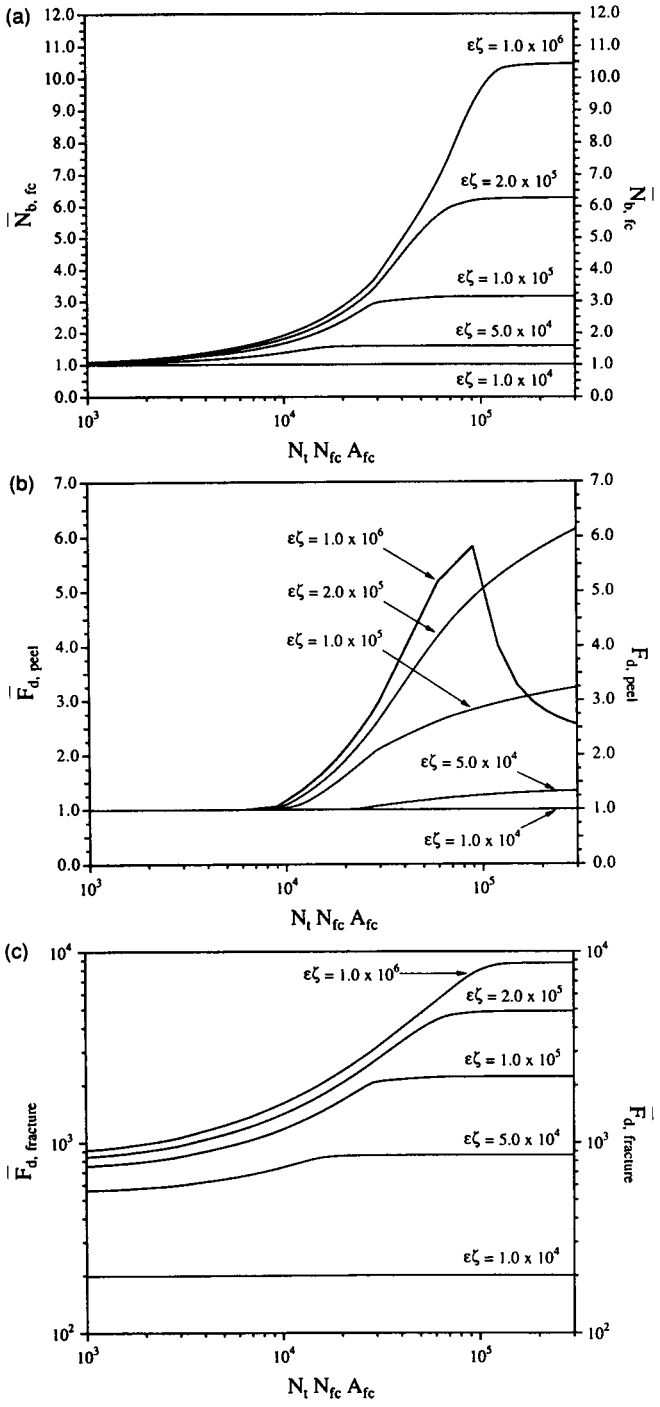

FIGURE 6 In these figures, we examine the influence of the talin and ligand densities on the extent of receptor clustering and the force to detach a focal contact-containing cell. The dimensionless bond density within the focal contact, $\bar{N}_{b,fc}$, and detachment force, $\bar{F}_d$, are plotted as functions of the dimensionless talin ($N_t N_{fc} A_{fc}$) and ligand ($\epsilon\zeta$) densities. (*a*) A minimum $\epsilon\zeta$ must be surpassed before significant receptor clustering within the focal contact occurs ($\bar{N}_{b,fc} > 1$). Clustering is maximal at elevated talin and ligand densities (*b*) Detachment through focal contact peeling is affected by receptor clustering. When clustering is negligible, there is no enhancement of the adhesive strength ($\bar{F}_{d,peel} = 1$), whereas at intermediate $\epsilon\zeta$, increases in the adhesive strength coincide with enhanced clustering. At high $\epsilon\zeta$ and $N_t N_{fc} A_{fc}$, diminished binding at the peeling edge leads to decreases in $\bar{F}_{d,peel}$. Peeling of the focal contact-containing cell may require forces six-fold higher than those necessary to detach a cell without focal contacts. (*c*) Because of the enhanced focal contact rigidity, fracture substantially ($>10^2$-fold enhancement) augments the adhesive strength even when clustering is negligible. Parameters are the same as in Fig. 3 and $\omega = 100$, $\alpha_{fc} = 0.03$, $\omega_{fc} = 100$, and $\psi_{fc} = 1$.

This section clearly demonstrates how a cell might control adhesive behavior through intracellular regulation of talin expression and receptor-talin avidity during adhesion and spreading.

Because substantially greater forces are required to detach focal contact than non-focal contact regions, it is relevant to compare the tensions generated during peeling or fracture to those necessary to lyse lipid bilayers (1–15 dyn cm^{-1}, Evans and Needham, 1986; Evans et al., 1976) to determine if detachment through membrane failure is possible in either case. The maximum dimensional tensions required to peel the focal contact are typically <0.2 dyn cm^{-1}, while we estimate that tensions of 0.2–7.0 dyn cm^{-1} are generated during fracture. One would therefore expect membrane rupture to be a signature of focal contact rigidity and fracture.

Following initial adhesion to fibronectin, fibroblasts and glioma cells exhibit increased coupling between adhesion receptors and cytoskeleton with a concomitant enhancement of the attachment strength (Lotz et al., 1989). Additionally, several researchers have shown that motile cells possess relatively few focal contacts, whereas stationary cells have an abundance of these adhesions (Kolega et al., 1982; Izzard and Lochner, 1980; Couchman and Rees, 1979). The number of focal contacts appears to be an important determinant of cellular adhesive behavior, consistent with the possibility that motile cells have an intermediate level of adhesiveness which simultaneously provides for traction and motion (DiMilla et al., 1991).

We examine the effect of the extent of focal contact formation on adhesive strength in Fig. 8 *a*, in which the dimensionless peeling force, $\bar{F}_d$, is plotted as a function of the fraction of the contact area occupied by focal adhesions, $2\alpha_{fc}/\alpha$, and the dimensionless receptor-talin affinity, ω_{fc}. Adhesive strengthening ($\bar{F}_d > 1$) occurs only after a minimum number of focal contacts are formed. The focal contact area required for strengthening when ω_{fc} is low can be quite substantial (almost 10% of the total contact area), whereas far fewer focal contacts are required at high receptor-talin affinities. Additionally, the detachment force exhibits a maximum at an optimal focal contact number. When $2\alpha_{fc}/\alpha$ is small, increased focal contact formation (increasing α_{fc}) leads to greater detachment forces; however, further increases in α_{fc} beyond the optimum value result in diminished attachment strengths. Increasing the total number of focal contacts increases the number of focal contacts which must be peeled at the cell margin, but reduces the bond density inside each focal contact since the same number of receptors are now distributed over more contacts. At low

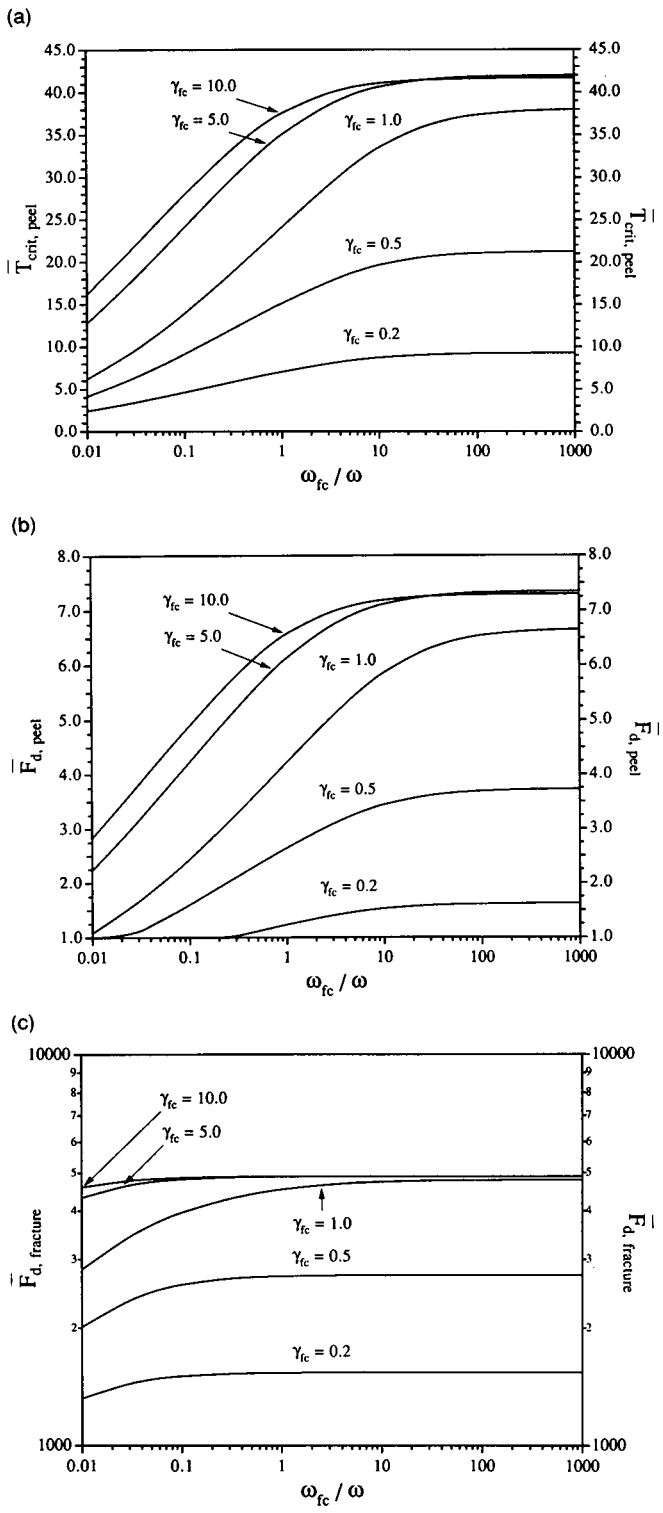

FIGURE 7 (*a–c*) Effect of receptor-talin affinity and talin density on the adhesive strength of focal contact-containing cells. (*a*) The dimensionless critical tension to peel a focal contact, $\bar{T}_{crit}$, increases with dimensionless affinity, ω_{fc}, and with dimensionless talin density, γ_{fc}, at low ω_{fc}. Diminished binding at the edge of contact results in a slight reduction in $\bar{T}_{crit}$ with increasing γ_{fc} at high ω_{fc}. (*b*) Detachment through focal contact peeling may require forces seven times higher than those necessary to detach a cell without focal contacts. (*c*) Fracture requires forces 1,000-fold greater than peeling, even at low ω_{fc} or γ_{fc}. Parameter values are identical to those in Fig. 6 except $\epsilon = 20$.

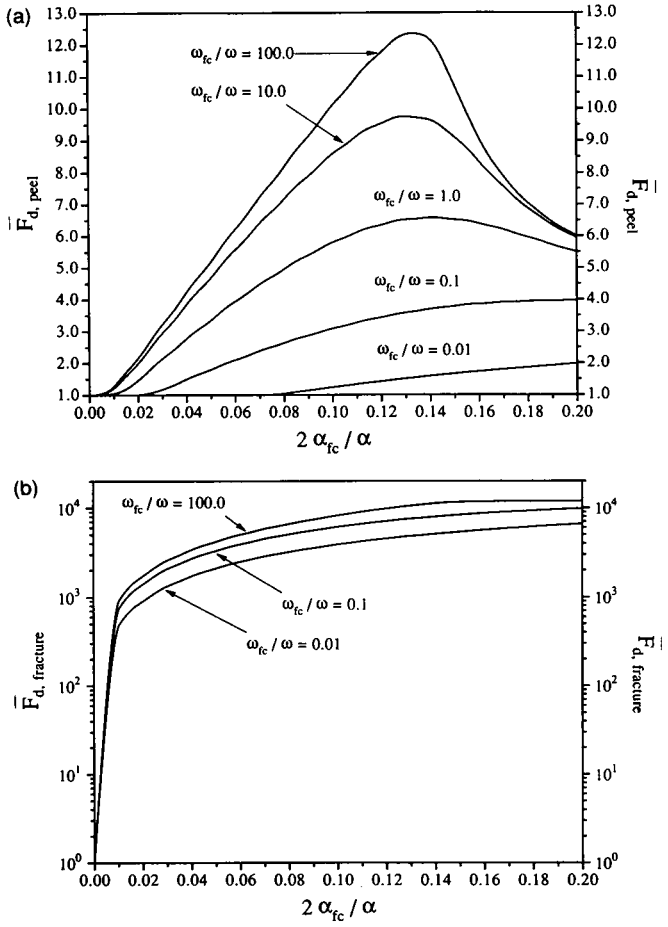

FIGURE 8 A plot of the dimensionless force to peel or fracture a focal contact-containing cell versus the dimensionless focal contact area, $2\alpha_{fc}/\alpha$, for different values of the dimensionless receptor-talin affinity, ω_{fc}/ω. (*a*) $\bar{F}_{d,peel}$ exhibits a biphasic response with increasing focal contact number (increasing $2\alpha_{fc}/\alpha$) such that an optimum focal contact number yields a maximum detachment force. (*b*) For fracture, focal contact formation always enhances the attachment strength, and only a few focal contacts are required to substantially increase the required detachment force. Parameter values are $\alpha = 0.7069$, $\beta = 27.4$, $\gamma_{fc} = 1.0$, $\delta = 10^{-3}$, $\epsilon = 20$, $\omega = 50$, $\phi = 2.25 \times 10^6$, $\psi_{fc} = 1.0$, and $\zeta = 1.125 \times 10^4$.

$2\alpha_{fc}/\alpha$, the increase in focal contact number dominates, and adhesion strength increases; at high $2\alpha_{fc}/\alpha$, the reduction in bond density dominates, and adhesion strength decreases. In the limit $2\alpha_{fc}/\alpha \rightarrow 1$, all bonds are equally distributed over the adhesive contact such that clustering is no longer possible and the force to peel a focal contact-containing cell will equal the force to detach a cell which lacks focal adhesions ($\bar{F}_d = 1$).

When the focal contact is mechanically rigid, increases in focal contact formation always require greater fracture forces (Fig. 8 *b*) since the enhanced focal contact rigidity dominates over the reduction in bond density within the focal contact. In addition, a >500-fold enhancement in attachment strength can be accomplished with relatively few focal contacts.

The disparity in adhesive strengthening between the peeling and fracture models is the assumed increase in the structural rigidity of the focal contact, but we have found the gap between these limits can not be bridged by increases in the effective membrane bending modulus. Increases in this parameter have no effect on the force to peel a focal contact (results not shown). The difference between peeling and fracture can be explained in terms of a characteristic length, τ, over which receptor-ligand bonds within the focal contact are stressed: increasing focal contact stiffness leads to larger τ and greater detachment forces. During peeling, $\tau \ll L_{fc}$ since only those bonds at the edge of the focal contact are under stress. In contrast, all receptor-ligand bonds are stressed simultaneously during fracture such that $\tau = L_{fc}$. Although enhanced bending rigidity increases τ in the peeling model, τ never becomes appreciable compared to the length of the focal contact, and the forces required for peeling remain considerably less than those for fracture.

COMPARISON WITH EXPERIMENT

The results of this paper demonstrate how cell adhesion might be influenced by receptor upregulation, enhanced secretion of adhesive ligands, or alterations in receptor-ligand affinity either in the presence or absence of focal contact formation. In this section, we examine how the predictions of this paper might be experimentally verified, and we make a detailed comparison between our theory and published experimental data in which adhesion strength and close contact formation have been correlated.

Recent advances in the development of biomaterials enable one to vary and quantify the density of adhesive ligands on a chemically-modified glass surface (Massia and Hubbell, 1990; Cozens-Roberts et al., 1990). Also, micropipet aspiration can be used to measure membrane tension, contact angle, and adhesive contact area (Evans, 1985*a*). Combination of these techniques in a well defined experiment may therefore allow one to test the theoretical predictions concerning the effect of ligand density on the minimum tension necessary to initiate detachment.

For example, our model predicts the critical tension will depend linearly on the ligand density, N_l, when N_l is much lower than the receptor density, R_t/A_{cell}, and be independent of N_l when $N_l \gg R_t/A_{cell}$ (Fig. 3 *a*). There are two direct ways of testing this prediction. First, a measurement of adhesion strength as ligand density is varied from low to high values should reproduce Fig. 3 *a*. Alternatively, one could examine this prediction using transfected cells which express different amounts of cell-surface adhesive receptors. A useful tool for these experiments are recently developed mutant fibronectin receptors which are expressed on the cell surface, bind extracellular ligand, but fail to localize in focal adhesions (Reszka et al., 1992; Marcantonio et al., 1990). These mutants would allow one to study the influence of ligand density and receptor expression on attachment strength in the absence of focal contact formation.

Predictions on the effect of receptor-ligand affinity in the absence of focal contact formation (Fig. 5) can also be tested; these experiments would involve modification of substrate chemistry. Binding assays reveal that the fibronectin receptor has a greater affinity for intact fibronectin than for RGD-containing peptides[1] (Akiyama and Yamada, 1985). Additionally, the conformation of the adhesive peptide may influence affinity; cyclic RGD-containing peptides are more efficient at inhibiting cell adhesion to extracellular matrix molecules than the linear variants (Aumailley et al., 1991; Kumagai et al., 1991). Measurement of the critical tension for cell adhesion on substrates made with these different ligands should enable one to test the predictions of Eqs. 14 and 17: the critical tension depends logarithmically on the receptor-ligand affinity at low ligand densities but is independent of affinity at high N_l.

Experimental verification of our results concerning the effect of altered receptor-cytoskeletal interactions on adhesive strength should be possible. Mutagenesis of the β_1 cytoplasmic domain of the fibronectin receptor has revealed that specific amino acid sequences within this domain can regulate receptor localization to focal contacts (Reszka et al., 1992; Marcantonio et al., 1990). Using mutant receptors which have slightly different cytoplasmic domains, it would be possible to vary the degree of interaction between receptor and cytoskeleton. In this manner, one may examine how receptor-talin affinity influences adhesive strength (Figs. 7 and 8). The most dramatic comparison would be to use cells which have been transfected with either wild-type receptors containing the entire β_1 subunit or mutant integrins in which the β_1 cytoplasmic domain has been completely removed. With this system, one could directly compare the adhesion strengths of cells which could (wild-type) and could not (mutant) form focal contacts. Finally, introduction of exogenous talin molecules into cells might enable one to test predictions concerning the effect of talin density on attachment (Figs. 6 and 7), although there may be other cytoskeletal factors which modulate the amount of talin incorporated into focal contacts.

It has been well documented that transformed cells exhibit fewer focal adhesions than normal phenotypes, possibly the result of reduced secretion of fibronectin or increased proteolysis of this protein (Burridge et al., 1988; Chen et al., 1986). Fibronectin receptors isolated from transformed cells display a reduced affinity for the cytoskeletal molecule talin (Tapley et al., 1989), providing an alternative explanation for diminished focal contact formation. The effects of these changes are clearly observed in adhesion studies, which have demonstrated that transformed cells are more rounded and less adher-

[1] RGD is the peptide sequence within fibronectin which is recognized by the fibronectin receptor and is capable of supporting cell adhesion.

ent than their normal counterparts (Burridge et al., 1988), although detailed quantitative analysis has not been pursued. Our model provides a robust theoretical framework to account for the disparate attachment strengths of normal and transformed cells: the model suggests reasons for the difference in adhesion strength might be lower ligand density, or weaker receptor-ligand or receptor-cytoskeletal interactions.

In addition to the predictions regarding the increase in adhesive strength of cells which can form focal contacts, the peeling and fracture models also predict different functionalities. In the peeling model, for example, there is an optimal number of focal contacts yielding a maximum attachment strength, which for the parameters chosen, occurs when focal contacts occupy ~13% of the total contact area. No such optimum exists if the focal contact fractures. It is quite interesting to note that analysis of published immunofluorescent micrographs reveals that focal contacts occupy ~5–15% of the contact area of well-spread cells. However, whether this represents an optimal focal contact number or a fortuitous coincidence is uncertain.

Recent work by Massia and Hubbell (1991) has demonstrated that human skin fibroblasts fail to form focal contacts when the density of RGD-containing peptide on the substrate is below 6×10^9 cm^{-2}. We predict large increases in the aggregation of integrin receptors (i.e., focal contact formation) require ligand densities above a critical value ($\epsilon\zeta > 10^4$, Fig. 6 *a*). In agreement with this prediction, Massia and Hubbell estimate the fibroblast-substrate contact area to be ~2,000 μm^2 which, for their reported ligand density of 6×10^9 cm^{-2}, gives $\epsilon\zeta = 3.8 \times 10^4$. In contrast, focal contacts were not observed when the ligand density was an order of magnitude lower ($\epsilon\zeta < 10^4$).

As mentioned previously, it is necessary to precisely identify the number and location of focal contacts in order to compare theory to experiment. Although Tözeren and coworkers (1992) quantified the adhesion strength of Jurkat cells to LFA-3-coated surfaces of known density using micropipet aspiration, they did not measure focal contact or cytoskeletal involvement in the cell-substrate interface; therefore, it is not possible to determine whether focal contacts were present in these cells, and thus is difficult to compare our model to these experiments.

Interference reflection microscopy (IRM) and total internal reflection fluorescence (TIRF) are often used to assess focal contact formation. In IRM, interference patterns of reflected light are used to determine cell-substrate separation distance (Izzard and Lochner, 1976). Closer separations appear dark, whereas longer distances are gray. Using this technique, focal contacts are identified as dark streaks which have a characteristic cell-substrate separation of 10–15 nm. Close contacts are thought to be weaker attachments since they appear as gray regions and thus represent longer separations (30–100 nm). In TIRF, a collimated light beam is directed into a microscope slide on which cells have been allowed to adhere (Gingell et al., 1985; Axelrod et al., 1983). Provided the correct incident angle, θ_i, is chosen, the beam will be totally, internally reflected within the microscope slide. An electromagnetic disturbance propagates into the cell-containing medium and is capable of exciting fluorescent molecules which are within a critical distance of the substrate. Since the decay length of the electromagnetic field depends on θ_i, varying θ_i allows one to accurately map the cell-substrate interface topography. TIRF has been successfully applied to identify focal contacts in chick heart explant cells (Gingell et al., 1985).

IRM and TIRF studies suggest that focal contacts are much stronger attachments than close contacts due to the smaller cell-substrate separation distance within focal contact regions. Consistent this hypothesis, immunofluorescent staining of adhesion receptors indicates that the majority of receptors are aggregated within focal contacts while few receptor-ligand bonds exist in close contacts (Fath et al., 1989; Duband et al., 1988; Dejana et al., 1988). Since there are sparse molecular cross-bridges in close contacts, these regions are not constrained to short separations, offer little resistance to applied forces, and provide a minor contribution to the adhesive strength compared to focal contacts.

One serious limitation to using IRM to identify focal contacts is that dark images at the cell periphery may be the result of reflections from the dorsal side of the lamella and thus not represent tight adhesive contact. Unfortunately, it is in precisely these same regions where focal contacts predominantly form (DePasquale and Izzard, 1991), thereby further complicating interpretation of IRM images. No such complication results from TIRF; because the electromagnetic wave decays exponentially, the fluorescent signal is highly sensitive to separation distance, enabling one to accurately map the cell-substrate interface topography, even at the cell periphery (Gingell et al., 1985). Unfortunately, in practice IRM is much simpler to implement than TIRF.

Although IRM and TIRF are useful for measuring cell-substrate separations, neither technique provides information as to the location of receptor-cytoskeleton linkages. Such knowledge can only be ascertained from immunofluorescent staining of cytoskeletal proteins and cell-surface receptors. For example, several studies suggest that 15–35% of the adhesive contact area is within close proximity to the substrate (Lotz et al., 1989; Harris, 1973; Abercrombie, 1971), whereas cytoskeletal involvement in focal contacts is limited to 5–15% of the total contact area (see Model Analysis section). Additionally, while mature focal contacts may be readily identifiable by IRM, it is unclear whether one may be able to consistently discern nascent attachments using this technique. Therefore, to unequivocally identify focal contacts or precursors to these attachments, it is necessary to use IRM or TIRF in conjunction with immuno-

TABLE 3 **Data for glioma cell adhesion to fibronectin***

Time	Temperature	Total adhesive contact area	Adhesive contact area <15 nm from substrate	Detachment force
min	*°C*	*μm^2*	*μm^2*	*$\mu dyn/cell$*
0	4	236 ± 31	1.1 ± 0.2	13–30
15	4	376 ± 49	13.4 ± 4	30
15	37	599 ± 175	138 ± 34	≥360

* Data taken from Lotz et al. (1989).

fluorescent staining of cytoskeletal proteins and adhesion receptors.

Of the many studies examining the formation of cell-substrate contacts, one study in particular, performed by Lotz and co-workers (1989), has examined the relation between reorganization of cell-substrate contacts and attachment strength. In this study, the adhesive strength of glioma cells on a fibronectin-coated surface was quantified using a centrifugation assay, while IRM was utilized to measure the contact area which was either ≤15 nm (hereafter referred to as 15 nm area) or between 15–100 nm from the substrate. The main results of this study are given in Table 3 and briefly discussed here. Initially, the glioma cells adhere to the fibronectin surface but form few contacts within 15 nm of the substrate. The force to detach 50% of the cells at 4°C is in the range of 13–30 μdyn/cell. Following a 15-min incubation on the fibronectin surface at 4°C prior to centrifugation, a ten-fold increase in the 15 nm area was observed; however, the strength of adhesion was unchanged from its initial level. After a 15-min incubation at 37°C, a substantial increase (>100×) in the 15 nm area was accompanied by over an order of magnitude enhancement in the required detachment force.

Normally, cell-substrate separations of ≤15 nm are characteristic of focal contacts. However, the ≤15 nm contacts observed in the glioma cell experiments described by Lotz and coworkers do not appear to be focal contacts in the strictest sense. Focal contacts are very tight, discrete regions of ≤15 nm separation in which receptors and cytoskeletal molecules cluster, whereas the contacts Lotz and colleagues identify appear much more diffuse. Cytochalasin can eliminate the strengthening response (Lotz et al., 1989), suggesting the enhancement in adhesion strength, which coincides with sizable increases in the 15 nm area, is the result of receptor clustering, cytoskeletal-receptor interaction, or both within these contacts. These initial ≤15 nm contacts appear to be precursors to mature focal contacts, since they are eventually resolved into "focal contacts" (Dr. David McClay, personal communication). Furthermore, in interpretation of their own experiments, Lotz and colleagues claim the adhesive strengthening is likely due to either clusters of ≈40 receptors per contact, or some combination of receptor clustering and cytoskeletal cross-linking (Lotz et al., 1989; Dr. David McClay, personal communication).

Considering all of the above evidence, we feel it is conservative to treat contacts ≤15 nm as precursor focal contacts which involve some degree of receptor clustering and receptor-cytoskeletal involvement. IRM by itself, without immunofluorescent staining of receptors or cytoskeleton, does not allow us to ascertain whether these contacts are uniformly or discretely located about the cell periphery. The analysis we present in this paper is sufficiently robust to treat either uniform or discrete clusters, so we shall employ the analysis in these two limits to cover all morphological possibilities for these contacts. We shall see that despite uncertainty in the details of contact morphology, our analysis can distinguish whether these cells detach through peeling or fracture.

Many of the parameters in our model have been experimentally determined for the glioma cell-fibronectin system or similar ones and are listed in Table 1. For example, there are in vitro measurements of the fibronectin-fibronectin receptor affinity (Akiyama et al., 1990) as well as the talin-fibronectin receptor affinity (Horwitz et al., 1986). Parameters which were not accurately quantified in the glioma cell-fibronectin study include the total cell area, the number, size and location of discrete ≤15 nm contacts, the fibronectin surface density, the total number of fibronectin receptors per glioma cell, and the talin density.

Following numerous simulations, we find that our results are not affected by changes in total cell area and thus assume $A_{cell} = 2{,}000\ \mu m^2$. When examining the possibility that ≤15 nm contacts are discrete precursor focal contacts, we assume these contacts are identical and are similar in size ($1\ \mu m^2$) to mature focal adhesions. We use the experimental measurements of 15 nm area as a first approximation to determine the number of discrete contacts within the adhesive region and assume that 70% of these contacts are located at the cell margin.

Based on the total number of fibronectin molecules placed in a single well in the glioma cell adhesion experiments, the maximum possible fibronectin surface density is $\sim 4.2 \times 10^{12}\ cm^{-2}$ (Lotz et al., 1989). Because studies on the adsorption of fibronectin to plastic and glass have reported a maximum fibronectin density in the range $0.9\text{–}3.0 \times 10^{12}\ cm^{-2}$, corresponding to a monolayer of fibronectin molecules (Hynes, 1990; Jones et al., 1986), we feel a ligand density of $10^{12}\ cm^{-2}$ is a reasonable best estimate of the true fibronectin density.

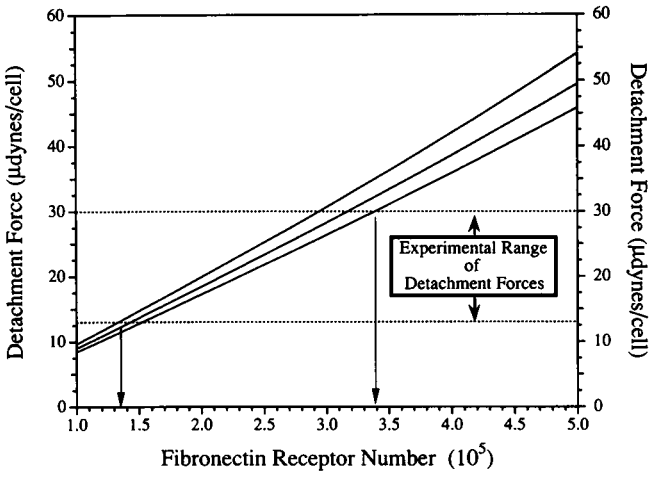

FIGURE 9 Comparison of model (*solid lines*) to the data of Lotz et al. (1989) for the initial adhesion of glioma cells to fibronectin at 4°C. Since the initial adhesion occurs in the absence of focal contacts, the only independent model parameter is the number of fibronectin receptors per glioma cell. Shown is a plot of detachment force versus receptor number for the experimentally measured minimum, mean, and maximum contact areas. The model accurately predicts the observed detachment forces when the receptor number is in the range 1.4–3.4 × 10^5, consistent with the number of fibronectin receptors on other cell types (Akiyama et al., 1990). Parameters are $A_{cell} = 2 \times 10^{-5}$ cm^2, $B = 10^{-12}$ ergs, $k_b\Theta = 3.8 \times 10^{-14}$ ergs, $K_{eq} = 5 \times 10^{-9}$ cm^2, $L = 8.08$, 8.67, and 9.22×10^{-4} cm, $N_l = 10^{12}$ cm^{-2}, $\lambda = 1.5 \times 10^{-6}$ cm, and $\kappa = 1$ dyn cm^{-1}.

The two remaining unknown parameters, the receptor number and talin density, are determined from comparison of our model to the initial and 15 min/4°C adhesion data, respectively. Then, comparison of our model to the data at 37°C should reveal whether peeling or fracture better describes the detachment of specific glioma cell adhesions.

Since adhesive strengthening is only observed when the temperature is raised from 4° to 37°C, we must address the influence of temperature on adhesion. Changes in temperature may affect adhesive behavior through alteration of membrane mechanical properties, kinetic parameters, or cellular metabolic rates. These issues are discussed in Appendix C.

The comparison of our model to the experimental data for the initial adhesion of glioma cells to fibronectin is shown in Fig. 9. Since less than 1% of the total adhesive contact area is within 15 nm of the substrate, we assume this initial attachment occurs in the absence of focal contact formation. In this case, adhesion is mediated solely by receptor-ligand binding and, since interactions with talin are not important, the only independent model parameter is the total number of fibronectin receptors per glioma cell. Fig. 9 demonstrates the dependence of the predicted detachment force on receptor number. Due to experimental variability in the adhesive contact area, we calculate a range of receptor numbers which satisfactorily match the observed detachment force of 13–30 μdyn. The model predicts 1.4–3.4 × 10^5 fibronectin receptors per glioma cell, a range which is consistent with the number of fibronectin receptors on other cell types (Akiyama et al., 1990). Although the receptor-ligand affinity at 4°C may be substantially higher than the reported affinity due to the influence of temperature on binding parameters (see Appendix C), we find that increases in affinity do not affect the predicted receptor number range (results not shown).

Significant increases in the 15 nm area occur during the 15-min incubation on fibronectin at 4°C, indicating that attachment sites involving cytoskeletal cross-linking and receptor clustering may be forming. Since talin rapidly (<10 min) aggregates near the cell membrane following substrate attachment (Beckerle et al., 1989; Mueller et al., 1989) and associates with precursors of mature focal contacts (DePasquale and Izzard, 1991), it is quite possible that the increase in 15 nm area is the result of initiated formation of focal contact precursors. In this case, we compare the detachment forces predicted by the peeling and fracture models to the observed forces. The uncertainties in the experimental measurements of total contact area and 15 nm area, as well as in the receptor number we have deduced from experiment, must be incorporated in our comparison, and will be reflected in uncertainty in the talin density derived by matching the data. As we shall see later in a detailed comparison to the 15 min/37°C data, our results for adhesion force are quantitatively comparable regardless of whether the ≤15 nm contacts are discretely or uniformly distributed. Thus, for purposes of determining an approximate talin density, we shall assume discrete ≤15 nm contacts. By plotting the predicted detachment force versus talin density and comparing these forces to those measured following the 15 min/4°C incubation, we obtain an acceptable range of talin densities.

We present the comparison of the fracture and peeling models to the 15 min/4°C adhesion data in Fig. 10. Even at the lowest talin densities, fracture requires detachment forces which are considerably (>100 times) larger than the reported values. The forces necessary to peel the discretely distributed ≤15 nm contacts are in better agreement with the experimental data. In fact, for talin densities between 2–5 × 10^{11} cm^{-2}, the peeling forces are identical to the experimentally measured detachment forces. While increases in the receptor-ligand affinity (due to lower temperatures) does not change this range, enhancement of the receptor-talin affinity results in a slightly narrower and lower range of acceptable talin densities (e.g., a 20-fold enhancement of K^t_{eq} yields N_t = 1.5–3.0 × 10^{11} cm^{-2}). These talin densities are reasonable and close to those estimated based on the results of Feltkamp and co-workers (1991), which were in the range 1.75 ± 0.68 × 10^{11} cm^{-2}.

Through comparison of our model to the 0 min/4°C and 15 min/4°C data, we have deduced ranges for receptor number (R_t) and talin density (N_t). However,

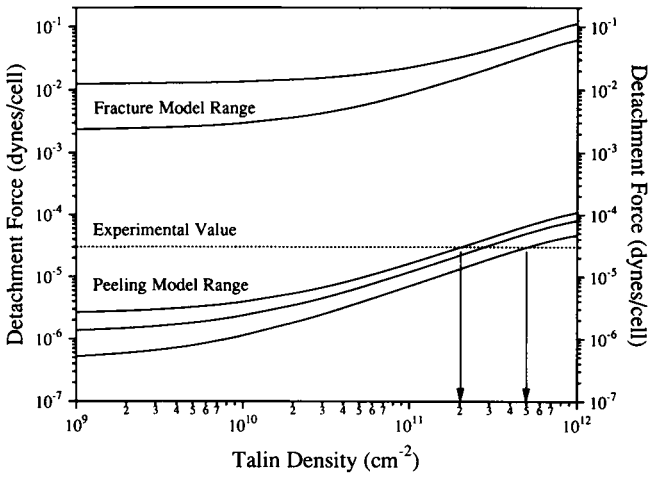

FIGURE 10 Comparison of model (*solid lines*) to the adhesion data (*dashed line*) for glioma cells incubated on a fibronectin-coated surface for 15 min at 4°C (Lotz et al., 1989). During this incubation, formation of precursors to mature focal contacts may be initiated since a significant fraction of the cell is within 15 nm of the substrate following incubation. In this case, it is relevant to compare the peeling and fracture models to experiment. Using the receptor number range determined in Fig. 9, we plot the detachment force versus the talin density, which is the only remaining independent parameter. Shown are the ranges of detachment force predicted by precursor focal contact peeling and fracture. Although fracture greatly overestimates the detachment force, the peeling model predicts that talin densities of $2\text{–}5 \times 10^{11}$ cm^{-2} will yield forces consistent with experimental observations. Additionally, these talin densities are close to those estimated ($1.75 \pm 0.68 \times 10^{11}$ cm^{-2}) from published electron micrographs of the talin distribution in focal contacts (Feltkamp et al., 1991). Parameter values are given in Fig. 9 except for $L = 1.02\text{–}1.16 \times 10^{-3}$ cm, $N_{fc} = 9\text{–}13$, and $R_t = 1.4\text{–}3.4 \times 10^5$.

since the fibronectin surface density was not directly measured, we examine how variations in ligand density affect our predicted ranges for R_t and N_t. We find that while a ligand density of 5×10^{11} cm^{-2} produces detachment forces and ranges for R_t and N_t close to those calculated when $N_l = 10^{12}$ cm^{-2}, further reduction in N_l drastically alters the results of our comparison to the experimental data of Lotz and colleagues (1989) (results not shown). At a ligand density of 10^{11} cm^{-2}, our model can still predict the initial level of adhesive strength for glioma cell adhesion to fibronectin, but fails to match the 15 min/4°C data. Based on these results, we would expect maximum glioma cell adhesion to occur at fibronectin densities $\geq 5 \times 10^{11}$ cm^{-2}, while densities below this value will lead to diminished attachment strengths.

At this point, there are no remaining adjustable parameters in the analysis, all unknown parameters having been measured or deduced by comparison of the theory to experiment. We now compare the forces predicted by peeling and fracture of $\leq$15 nm contacts to the strengthening response at 37°C (Fig. 11). Although Lotz and colleagues (1989) report the 15 nm area occupied ~25% of the total contact area following the 15 min/37°C incubation, analysis of immunofluorescent micrographs from other cell systems reveals that mature focal contacts typically occupy only 10% of the total contact area, suggesting the cited 15 nm area might overestimate precursor focal contact area. We therefore compare the peel-

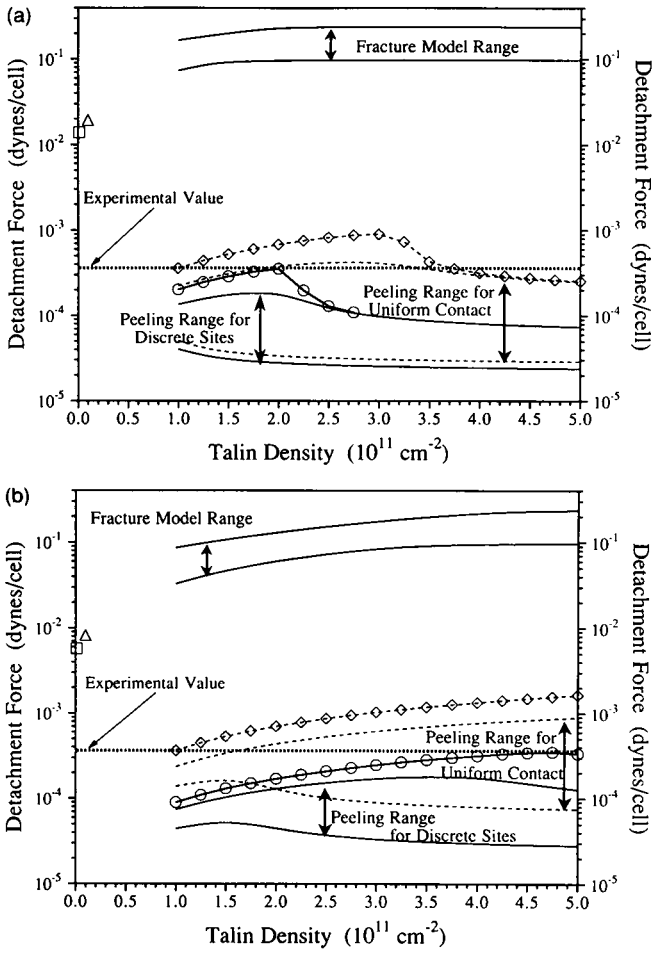

FIGURE 11 Comparison of model (*solid and dashed lines*) to the data of Lotz et al. (1989) for the strengthening of glioma cell attachment to fibronectin at 37°C (*heavy dashed line*). For this comparison, all model parameters are known or have been deduced from Figs. 9 and 10. Fig. 11 *a* compares the peeling and fracture forces assuming there is a one-to-one correspondence between the area of receptor clusters and the reported 15 nm area, whereas in Fig. 11 *b*, we assume that the extent of cytoskeletal cross-linking of adhesion receptors occurs over only 10% of the measured total contact area. For each of these cases we compare the range of forces required to detach a cell through peeling when receptor-cytoskeleton interactions are either confined to discrete attachment sites, modeled as precursor "focal contacts" (*solid lines*), or spread over a uniform contact region extending around the cell periphery (*dashed lines*). Fracture overestimates the detachment force, even at reduced talin densities (□, $N_t = 10^9$ cm^{-2}; △, $N_t = 10^{10}$ cm^{-2}). The maximum detachment forces predicted for peeling of discrete focal contacts are within a factor of two of the observed force, whereas peeling of a uniform contact can require forces above the experimental value. A reasonable enhancement (100 times) in the receptor-talin affinity, presumably through biochemical modification of either the receptor or talin, yields maximum peeling forces equal to (⊖, discrete sites) or in excess of (◇, uniform contact) the experimentally measured value. Parameters are given in Figs. 9 and 10 except for $L = 1.16\text{–}1.57 \times 10^{-3}$ cm and $N_{fc} = 104\text{–}172$.

ing and fracture models to experiment for several different scenarios which span the range of possibilities for ≤15 nm contact distribution. Fig. 11 *a* compares the peeling and fracture forces assuming a one-to-one correspondence between precursor focal contact area and the reported 15 nm area, whereas in Fig. 11 *b*, we assume the precursor focal contact area is smaller, only 10% of the measured total contact area. Also in Fig. 11, *a* and *b*, we consider the case when an equivalent area (either 25 or 10% of the reported ≤15 nm contact region) is either localized in discrete contacts or uniformly distributed around the cell periphery. These simulations span the entire possible range of experimental interpretation (discrete vs. uniform contacts; peeling vs. fracture).

Lotz et al. (1989) proposed that detachment at 37°C occurred through detachment of clusters containing ≈40 receptors (corresponding to $N_t = 10^9$ cm^{-2}); we find the adhesive strengthening response can not be explained by focal contact fracture as this mode of detachment requires unreasonably large forces, even if our predicted talin density is in error by two orders of magnitude (Fig. 11, *a* and *b*). Additionally, the fracture forces for discrete contacts or a uniform contact are identical since the same number of bonds must be broken at the cell periphery in each case. Interestingly, we find the fracture force relatively insensitive to significant decreases in the extent of cytoskeletal cross-linking (compare Fig. 11, *a* and *b*). Since fracture consistently predicts detachment forces 15–100 times larger than the reported measurement, we conclude fracture overestimates the observed strengthening response at 37°C.

In contrast, the range of peeling forces agrees well with the experimental data. Although the peeling model predicts detachment forces slightly less than the measured value when attachment occurs in discrete locations (*solid lines*, Fig. 11, *a* and *b*), the maximum peeling force in this case is within a factor of two to the measured glioma cell adhesive strength, whether 10 or 25% of observed ≤15 nm contacts are focal. We consider this good agreement, given the uncertainty in parameters such as talin density and receptor-talin affinity, since there are no adjustable parameters in this comparison. Because the peeling force is proportional to the length of the peeling edge, attachment mediated by discrete contacts should provide a lower bound to the detachment force. In fact, when receptor-cytoskeletal contacts are uniformly distributed around the peeling edge, we find the maximum possible detachment forces slightly exceed the reported value (Fig. 11, *a* and *b, dashed lines*).

The receptor-talin affinity we have used in these comparisons was measured in an *in vitro* system and may therefore be considerably less than the *in vivo* avidity due to intracellular biochemical changes such as phosphorylation of talin, integrin receptors, or both (Burridge et al., 1988). In fact, large increases in avidity following receptor activation are not uncommon: both the gpIIbIIIa complex on platelets and the LFA-1 integrin on T-lymphocytes undergo substantial enhancements in affinity for their respective ligands following cellular activation (Dustin and Springer, 1989). Since it is quite reasonable to suggest that through phosphorylation or some other mechanism of molecular modification, the receptor-talin affinity is dramatically increased during the 37°C strengthening response, we examined the effect of avidity enhancement on the peeling forces. We demonstrate in Fig. 11 that large but not unreasonable increases (≥100×) in the receptor-talin affinity improve the match between the peeling model and the experimentally measured detachment force when cytoskeleton-induced receptor aggregation occurs in discrete contacts (Fig. 11, *a* and *b, circles*). For uniformly distributed cytoskeletal interactions, the same avidity enhancement further increases the maximum peeling forces beyond the reported value for glioma cell adhesion to fibronectin (Fig. 11, *a* and *b, diamonds*). Considering all of the calculations in Fig. 11, given the good agreement between theory and experiment without modulation of receptor-talin affinity and the very reasonable augmentation of adhesive strength by intracellular biochemical modification of receptor-talin interactions, it is our conclusion that the response of specific glioma cell attachment sites to centrifugational stresses is best described by peeling, rather than fracture, of the adhesive contact. However, our model does not allow us to determine whether areas reported as ≤15 nm contacts are actually discrete precursor focal contacts or a more diffuse clustering of receptors about the cell periphery.

SUMMARY

We have presented a mathematical treatment of receptor-mediated adhesion which allows us to quantify the contributions of receptor redistribution, membrane mechanics, and focal contact formation on adhesive strength. Two possible modes of focal contact detachment which represent vastly different responses to applied forces were examined: (*a*) progressive peeling of focal contacts lacking cytoskeletal mechanical rigidity and (*b*) fracture of all receptor-ligand bonds within a totally rigid focal contact. To our knowledge, this is the first analysis which incorporates focal contact formation in a mathematical study of cell adhesion.

In the absence of focal contacts, the adhesive strength depends on both the extent of binding and the membrane morphology at the edge of contact. We have derived analytic formulas for the critical tension necessary to initiate membrane peeling in the limits of low and high ligand density which differ from previous expressions (Dembo et al., 1988) since we have allowed the receptors to redistribute over the cell surface. We have also discussed how these theoretical predictions might be verified using carefully designed experiments.

Our analysis conclusively demonstrates that formation of cytoskeletal adhesive plaques can substantially augment the adhesive strength above the level attained in the absence of focal contacts. Whereas peeling of focal adhesions supports a maximum enhancement in the attachment strength of an order of magnitude, fracture of focal contacts may require forces 1000 times larger, and the tensions generated during fracture are comparable to tensions necessary for membrane rupture.

We have compared our analysis to an experimental study of glioma cell attachment to fibronectin which suggested that adhesive strengthening occurs with receptor clustering and cytoskeletal involvement at 37°C but not at 4°C (Lotz et al., 1989). Despite some difficulty in interpreting the contact morphologies in these cells, we chose to analyze this data because it is the only study we know in which contact morphologies and adhesion strength are correlated. We find that detachment through peeling can accurately describe the adhesion results at 4°C and, as further support to this hypothesis, our comparison at this temperature yields ranges in the number of fibronectin receptors per glioma cell and the talin density which are consistent with independent measurements for other cell types. For the adhesive strengthening response at 37°C, with no adjustable parameters, the peeling model predicts detachment forces which are comparable to the observed forces. In addition, differences between model and experiment diminish as the receptor-talin avidity is enhanced. These results suggest that although cytoskeletal cross-linking of fibronectin receptors significantly increases adhesion strength, specific glioma cell-substratum attachment sites possess little structural rigidity and detach through a peeling mechanism.

Due to experimental uncertainties involved with interpretation of IRM images, the observed strengthening of glioma cell adhesion to fibronectin can not be conclusively attributed to the formation of mature focal contacts. However it is still quite possible, and in fact it is the opinion of Lotz and colleagues (1989), that receptor-cytoskeleton interactions are involved in adhesive strengthening. The attachment strength of glioma cells after the 15 min/37°C incubation is greater than the initial adhesion but less than the adhesive strength after a one hour incubation, consistent with the interpretation that focal contact precursors are forming during the 15 min/37°C incubation. While the peeling model accurately describes the detachment of such precursors, mature glioma cell focal contacts may respond to applied stresses in a manner resembling fracture. Additionally, differences in cytoskeletal architecture may contribute to the variation in the adhesion strength between cell types. For example, although a detachment force of 360 μdyn/cell was sufficient to remove 50% of the glioma cells following adhesive strengthening at 37°C, fibroblasts do not detach from fibronectin at this force (Lotz

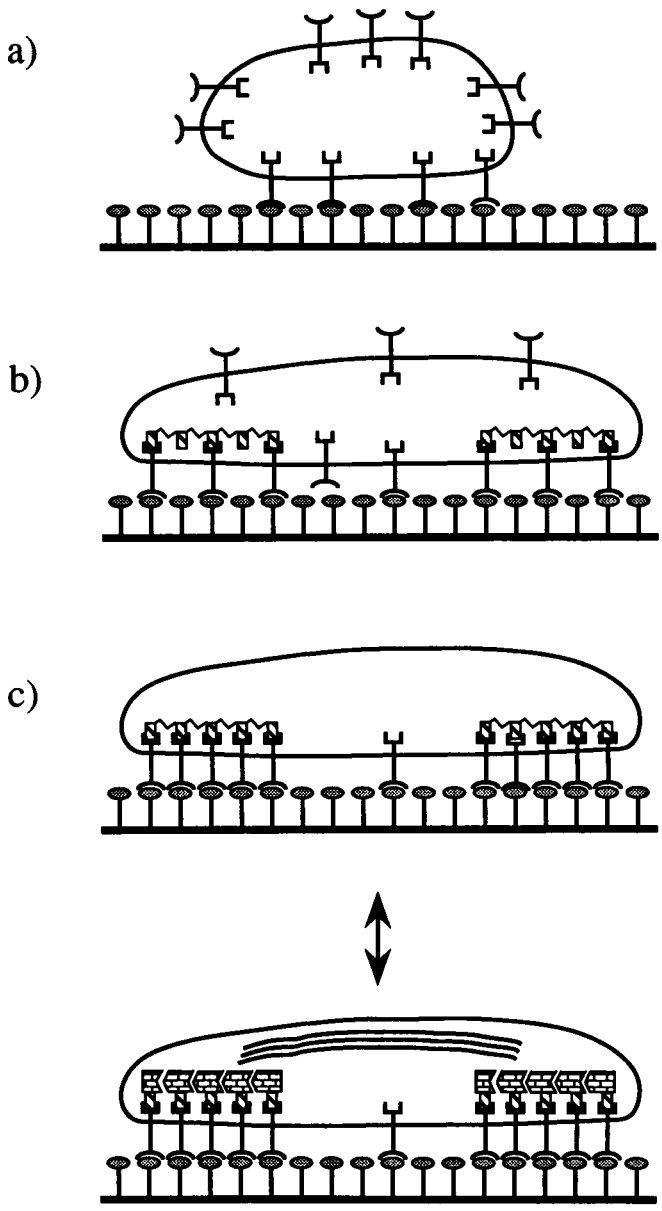

FIGURE 12 In order to explain the strengthening of receptor-mediated adhesion through cytoskeletal reorganization, we present a modified "stick and grip" model. (*a*) Initially, the cell adheres through the interaction of cell-surface receptors with extracellular ligand molecules. (*b*) Following the initial adhesion, talin-containing cytoskeletal precursors of the focal contact induce receptor clustering into localized areas within the adhesive contact. These precursors possess no mechanical rigidity and thus detach through peeling. (*c*) Strengthening of the focal contact attachment is energy dependent and may occur through a combination of enhanced receptor clustering and solidification of the focal contact structure, most likely involving linkage between focal contacts via actin filaments. The relative contributions of clustering and solidification will determine whether peeling or fracture most closely approximates the true detachment mechanism. Since the forces to peel or fracture the focal contact differ by several orders of magnitude, the extent of adhesive strengthening may be precisely controlled through intracellular modulation of receptor-cytoskeleton binding and focal contact rigidity, such that cell types which differ in ability to assemble and solidify focal contacts will exhibit markedly different attachment strengths.

et al., 1989) and may therefore possess focal contacts which are more rigid than those of glioma cells.

In order to describe the variability in adhesive strengthening response for different cell types, we propose a modified version of the "stick and grip" model of cell adhesion which considers the effect of focal contact stiffness on attachment strength (Fig. 12). Following initial attachment, which is presumed to occur through receptor-ligand binding, adhesion receptors may be clustered into localized patches at the cell periphery through cross-linking of their cytoplasmic tails by talin-containing precursors of the mature focal contact (Fig. 12 *b*). Experiments have verified the existence of such precursors (DePasquale and Izzard, 1991), but have not determined the microstructure of these sites. Supposing these precursors consist of a loose network of cytoskeletal molecules which possess little mechanical stiffness, detachment of these specific attachment sites would occur through peeling and negligible adhesive strengthening would be observed. Increased assembly and strengthening of individual focal attachments is an active process and may involve a combination of enhanced receptor clustering and focal contact solidification (Fig. 12 *c*). While clustering may be affected by changes in the receptor-talin avidity or talin density, focal contact rigidity may be augmented through association with actin filaments or through reinforcement of the interactions between individual focal contact components. In this scenario, adhesion strength can be very sensitively controlled by intracellular biochemical changes such as talin expression or modulation of receptor-talin affinity, or through solidification of cytoskeletal linkages within the focal contact. The level of adhesive strengthening observed for a particular cell type depends on whether clustering or solidification is the dominant method of adhesive strengthening: as the extent of solidification increases, the mode of detachment moves from peeling toward fracture, and the adhesive strength increases accordingly. The strengthening response may also be influenced by the kinetic nature of the solidification process. Because cytoskeletal reorganization may be incomplete after 15 min, focal adhesions which have formed by this time are incapable of withstanding the same detachment force as the mature focal contact, which may require over an hour for complete assembly. Since different cell types may possess focal adhesions of intermediate levels of stiffness, future theoretical studies should examine focal contact structures between the peeling and fracture limits.

In its current form, our analysis is limited since we do not account for the effect of kinetic processes on adhesion and detachment. The time-dependent peeling of a membrane in the absence of focal contact formation has been studied (Dembo et al., 1988) and, while complex, a similar analysis incorporating focal adhesions should be feasible. A kinetic analysis of cell adhesion should also include the dynamics of focal contact formation, focussing on the accumulation of individual cytoskeletal components near the cell membrane, the subsequent solidification of this aggregate of molecules, and the influence of intermediate structures between precursor and mature focal contact on attachment strength.

An additional limitation is the absence of cellular deformation. For example, we have assumed that in the absence of focal contacts, the contact area remains constant as the ligand density increases. This assumption may not be valid since higher ligand densities can lead to greater attachment strengths which may support cell spreading. If one assumes that cell deformation is controlled by membrane mechanical properties, the adhesive contact area may be obtained through calculation of the membrane configuration which minimizes the mechanical energy of the system. Although this type of analysis would explicitly include the critical tension and therefore accompany our adhesion model quite well, it is an unrealistic model of cell spreading, which occurs through active processes including actin filament extension and cytoskeletal rearrangement. DiMilla and colleagues (1991) have recently developed a model which examines how cytoskeletal force generation affects cell migration and Dembo and Harlow (1986) have proposed a model of the cytoplasm as a reactive, contractile biological polymer network; these types of analyses would have to be incorporated in models of cell spreading to correctly account for cytoskeletal protrusive and contractile stresses. In this paper, we find that modeling the focal contact as a passive structure which balances externally applied detachment forces in the absence of active contractile forces can describe the adhesive strengthening phenomena resulting from focal contact formation. We note that any active contractile stresses which act tangentially or normally to the cell membrane can be incorporated within the formalism presented in this paper. This type of analysis might provide a useful description of cell motility where contractile and adhesive stresses are in balance, and externally applied forces are absent.

In summary, we have developed a mathematical model of receptor-mediated cell adhesion which quantitatively describes how upregulation of receptors, alteration of the receptor-ligand affinity through chemical modification, increased secretion of adhesive ligands, and focal contact formation affect attachment strength. This model allows us to understand how cells might modulate their adhesive behavior and will hopefully motivate further experimental studies to elucidate the important chemical, physical, and mechanical factors which influence cell adhesion.

APPENDIX A

The following analysis describes the dimensionless equations and numerical solution algorithm for the model in the absence of focal con-

tacts. For the focal contact extension of the model, the bond density equations are modified as discussed in Appendix B, while the bond density terms in the force balances and boundary condition at $s = 0$ are adjusted to account for the presence of the focal contact.

The governing nondimensional equations are obtained by defining the following scalings:

$$\bar{s} = \frac{s}{L}, \quad \bar{x} = \frac{x}{L}, \quad \bar{y} = \frac{y}{\lambda}, \quad \bar{C} = \frac{CL^2}{\lambda},$$

$$\bar{N}_b = \frac{N_b A_{cell}}{R_t}, \quad \bar{N}_f = \frac{N_f A_{cell}}{R_t}, \quad \text{and} \quad \bar{T} = \frac{TL^2}{B}.$$

Bond and receptor balance equations:

$$0 = \omega \bar{K}(\epsilon - \bar{N}_b)\bar{N}_f - \bar{N}_b \tag{A1}$$

and

$$1 = \bar{N}_f + \alpha \int_0^1 \bar{N}_b \bar{x}\, d\bar{s}, \tag{A2}$$

where

$$\bar{K} = \exp\{-\beta(\bar{y} - 1)^2\}. \tag{A3}$$

Membrane mechanical equilibrium equations:

$$\frac{\partial^2 \bar{C}}{\partial \bar{s}^2} - \bar{C}\bar{T} = -\zeta\phi\left[\bar{N}_b(\bar{y} - 1)\frac{\partial \bar{x}}{\partial \bar{s}}\right] \tag{A4}$$

and

$$\frac{\partial \bar{T}}{\partial \bar{s}} + \left(\frac{\delta^2}{2}\right)\frac{\partial \bar{C}^2}{\partial \bar{s}} = \zeta\phi\delta^2\left[\bar{N}_b(\bar{y} - 1)\frac{\partial \bar{y}}{\partial \bar{s}}\right]. \tag{A5}$$

Arclength and curvature expressions:

$$\left(\frac{\partial \bar{x}}{\partial \bar{s}}\right)^2 + \delta^2\left(\frac{\partial \bar{y}}{\partial \bar{s}}\right)^2 = 1 \tag{A6}$$

and

$$\bar{C} = \left(\frac{\partial \bar{x}}{\partial \bar{s}}\right)\left(\frac{\partial^2 \bar{y}}{\partial \bar{s}^2}\right) - \left(\frac{\partial \bar{y}}{\partial \bar{s}}\right)\left(\frac{\partial^2 \bar{x}}{\partial \bar{s}^2}\right). \tag{A7}$$

Boundary and matching conditions:

While symmetry arguments require the membrane at $\bar{s} = 1$ to be continuous, energy considerations reveal that the most favorable geometry at this point is a flat interface with a separation distance equal to the unstressed bond length. Thus, at $\bar{s} = 1$, $\bar{y} = 1$ and $(\partial \bar{y}/\partial \bar{s}) = 0$.

Since binding is negligible in the macroscopic region, in order for continuity to be established between the microscopic and macroscopic regions, the separation distance at $\bar{s} = 0$ must ensure that the bond density at $\bar{s} = 0$, $\bar{N}_{b,\bar{s}=0}$, is sufficiently small so that binding stresses are much smaller than membrane tensions at this point. Although $\bar{N}_{b,\bar{s}=0}$ determines the separation distance at the contact periphery, our results, in particular the adhesive strength measurements, are insensitive to the particular choice of $\bar{N}_{b,\bar{s}=0}$. Finally, the membrane geometry and tension at the edge of the microscopic contact region must also be specified. At $\bar{s} = 0$, $\bar{C} = \bar{C}_{mic}$, $\bar{T} = \bar{T}_{mic}$, $(\partial \bar{y}/\partial \bar{s}) = -(\sin \theta_{mic}/\delta)$, and $\bar{y}$ is determined by $\bar{N}_b \le \bar{N}_{b,\bar{s}=0}$.

Although the values for the microscopic contact angle (θ_{mic}), curvature ($\bar{C}_{mic}$), and tension ($\bar{T}_{mic}$) are not known a priori, one can measure the macroscopic equivalents of these parameters. Solution of the membrane mechanical equilibrium equations in the macroscopic region yields relations between the macroscopic tension ($\bar{T}_{mac}$), curvature ($\bar{C}_{mac}$), and angle (θ_{mac}) and their microscopic counterparts (Dembo et al., 1988; Evans, 1985*a*, *b*):

$$\bar{T}_{mic} = \bar{T}_{mac}\cos(\theta_{mac} - \theta_{mic}), \tag{A8}$$

$$(\bar{C}_{mic})^2 = (\bar{C}_{mac})^2 + \left(\frac{2\bar{T}_{mac}}{\delta^2}\right)[1 - \cos(\theta_{mac} - \theta_{mic})], \tag{A9}$$

and

$$\frac{\partial \bar{C}_{mic}}{\partial \bar{s}} = \left(\frac{\bar{T}_{mac}}{\delta}\right)\sin(\theta_{mac} - \theta_{mic}). \tag{A10}$$

Solution of this nonlinear system of equations yields the membrane morphology as well as the bond density and tension as functions of membrane position. Since the solution depends on T_{mac} ($= T_{crit}$) and θ_{mic}, which are not known a priori, an iterative procedure is necessary.

We utilize a finite difference algorithm where the microscopic membrane region is divided into a one-dimensional grid. Because the membrane curvature is highest at the edge of contact, a finer mesh-size is employed in this region in order to minimize numerical errors. The iterative procedure is begun by providing estimates for T_{crit}, θ_{mic}, and the initial membrane shape. As a first approximation, $\bar{y}_{\bar{s}=0}$ is determined from solution of A1 assuming $\bar{N}_f = 1$. Using the initial morphology and Eqs. A1–A3, $\bar{N}_b(\bar{s})$ is calculated. Next, the tangential force balance Eq. A5 and the arclength expression A6 are numerically integrated to calculate $\bar{T}(\bar{s})$ and $\bar{x}(\bar{s})$. Simultaneous solution of the normal force balance A4 and curvature A7 equations yields the cell-substrate separation and membrane curvature. The new membrane shape is used to find improved estimates for the bond density, tension, and arclength. Following convergence of the membrane morphology, we check that Eq. A10 is satisfied. If it is not satisfied, a new estimate for the microscopic contact angle is made, the microscopic quantities are adjusted, and $\bar{N}_b$, $\bar{T}$, $\bar{x}$, $\bar{y}$, and $\bar{C}$ are updated. If A10 is satisfied, A5 is integrated to obtain a new estimate for the critical tension and the solution loop is repeated. Once the critical tension converges, the final step is to determine a new $\bar{y}_{\bar{s}=0}$, this time accounting for receptor depletion, and calculate the membrane morphology. The algorithm is completed when $\bar{y}_{\bar{s}=0}$ converges.

APPENDIX B

This section details the procedure used to calculate the bond densities in the focal contact model. Scaling all densities to R_t/A_{cell}, one obtains the following dimensionless equations:

$$N_{bo}: \quad 0 = \omega \bar{K}(\epsilon - \bar{N}_{bo})\bar{N}_f - \bar{N}_{bo}, \tag{B1}$$

$$N_{bi}: \quad 0 = \omega \bar{K}(\epsilon - \bar{N}_{bi} - \bar{N}_{bc})\bar{N}_f - \bar{N}_{bi} + \psi_{fc}\bar{N}_{bc} - \omega_{fc}\psi_{fc}(\epsilon\gamma_{fc} - \bar{N}_c - \bar{N}_{bc})\bar{N}_{bi}, \tag{B2}$$

$$N_c: \quad 0 = \omega_{fc}\psi_{fc}(\epsilon\gamma_{fc} - \bar{N}_c - \bar{N}_{bc})\bar{N}_f - \psi_{fc}\bar{N}_c + \bar{N}_{bc} - \omega\bar{K}(\epsilon - \bar{N}_{bi} - \bar{N}_{bc})\bar{N}_c, \tag{B3}$$

$$N_{bc}: \quad 0 = \omega\bar{K}(\epsilon - \bar{N}_{bi} - \bar{N}_{bc})\bar{N}_c + \omega_{fc}\psi_{fc}(\epsilon\gamma_{fc} - \bar{N}_c - \bar{N}_{bc})\bar{N}_{bi} - (1 + \psi_{fc})\bar{N}_{bc}, \tag{B4}$$

and

$$N_f: \quad \bar{N}_f = 1 - \bar{N}_{bo}\left(\frac{\alpha}{2} - \alpha_{fc}\right) - \alpha_{fc}(\bar{N}_{bi} + \bar{N}_c + \bar{N}_{bc}), \tag{B5}$$

where $\bar{K}$ is given by A3. Since the bond densities depend on $\bar{y}(\bar{s})$, this nonlinear system of equations must be solved at each grid point.

Because the majority of the membrane is flat except for a small boundary region at the edge of contact, we assume that $\bar{y} = 1$ for all $\bar{s}$ in order to obtain an approximate $\bar{N}_f$. Prior to the start of the main algorithm, Eqs. B1–B5 are solved simultaneously to determine the free receptor density, which is then treated as a constant for the remainder of the solution procedure.

Once $\bar{N}_f$ is calculated, B1 is easily solved to obtain $\bar{N}_{bo}$ at each membrane location outside the focal contact, while within the focal contact, B2–B4 are solved simultaneously to determine $\bar{N}_{bi}$, $\bar{N}_c$, and $\bar{N}_{bc}$ as functions of arclength.

APPENDIX C

In this section, we investigate how temperature changes affect the adhesive strength through alterations in membrane mechanical properties, binding affinity, and cellular metabolism.

For a thin, inextensible membrane, the resistance to membrane deformation will be governed by the bending modulus. Although temperature will affect membrane fluidity and thus bending rigidity, we have found that changes in the bending modulus, even of an order of magnitude, have a negligible influence on adhesive strength.

Since increases in temperature decrease the tension necessary for lysis of lipid bilayers (Evans and Needham, 1986), one would expect a higher incidence of membrane failure at 37°C than at 4°C. Substantial augmentation of the adhesive strength was observed only at 37°C, thus it is most relevant to address membrane material properties at this temperature. For red blood cells, lysis tensions do not change appreciably and are in the range 3–12 dyn cm^{-1} for temperatures between 25° and 50°C (Evans et al., 1976). While these tensions are comparable to those generated during focal contact fracture, comparison of model to experiment suggests that detachment at 37°C occurs through a peeling mechanism. We would therefore expect detachment through failure of the glioma cell membrane to be insignificant. Unfortunately, the extent of membrane lysis was not quantified in the adhesion experiments of Lotz and co-workers.

Since glioma cell adhesion was studied at 4° and 37°C, it is important to examine the effect of temperature on binding parameters. Decreases in temperature may influence bond formation through two opposing effects: a diminished forward binding constant and an enhanced affinity (Hammer and Lauffenburger, 1987). In our analysis, we consider binding at steady-state, and therefore need only examine the effect of temperature on receptor-ligand (or talin) affinity:

$$K_{R-L} = K_{eq} \exp\left\{\frac{-\kappa(y-\lambda)^2}{2k_b\Theta}\right\} \quad \text{and} \quad K_{R-T} = K'_{eq},$$

While it is obvious that temperature changes will affect the exponential term, since the equilibrium affinity can be related to the enthalpy and entropy of reaction,

$$K_{eq}\,(\text{or } K'_{eq}) = \exp\left(\frac{-\Delta G}{R\Theta}\right) = \exp\left(\frac{-(\Delta H - \Theta\Delta S)}{R\Theta}\right),$$

a reduction in temperature may also alter K_{eq} and K'_{eq}. In the above relation, ΔG is the free energy change of reaction, ΔH and ΔS are the enthalpy and entropy of reaction, respectively, and R is the gas constant. Using reasonable values for these parameters developed for antibody-hapten interactions (Pecht and Lancet, 1977), a change in temperature from 37° to 4°C may lead to a maximum 18-fold enhancement of the affinity, although typical increases may be closer to 5-fold. Thus, the effect of temperature on receptor-ligand and receptor-talin association can be investigated through changes in the appropriate binding affinity.

Since reorganization of the cytoskeleton is energy dependent, lower temperatures may inhibit the formation of focal contacts. At 4°C, the strengthening response may be delayed or prevented entirely if energy barriers to focal contact formation can not be overcome, whereas physiological temperatures will support cytoskeletal reorganization and focal adhesion development. Although we do not directly account for the time-dependent evolution of the focal contact, the peeling and fracture models depict different stages of focal adhesion maturation and the extent of focal contact formation is an input variable, such that the temperature effect on cytoskeletal restructuring is implicitly imbedded in our analysis.

This work was supported by a grant from the Cornell Biotechnology Program which is sponsored by the New York State Science and Technology Foundation, a consortium of industries, the United States Army Research Office, and the National Science Foundation, as well as a National Science Foundation grant to Daniel A. Hammer (BCS-9009506).

Received for publication 7 May and in final form 2 October 1992.

REFERENCES

1. Abercrombie, M., J. E. Heaysman, and S. M. Pergrum. 1971. The locomotion of fibroblasts in culture. *Exp. Cell Res.* 67:359–367.
2. Akiyama, S. K., K. Nagata, and K. M. Yamada. 1990. Cell surface receptors for extracellular matrix components. *Biochim. Biophys. Acta.* 1031:91–110.
3. Akiyama, S. K., and K. M. Yamada. 1985. Synthetic peptides competitively inhibit both direct binding to fibroblasts and functional biological assays for the purified cell-binding domain of fibronectin. *J. Biol. Chem.* 260:10402–10405.
4. Aumailley, M., M. Gurrath, G. Müller, J. Calvete, R. Timpl, and H. Kessler. 1991. Arg-Gly-Asp constrained within cyclic pentapeptides. Strong and selective inhibitors of cell adhesion to vitronectin and laminin fragment P1. *FEBS Lett.* 291:50–54.
5. Axelrod, D., N. L. Thompson, and T. P. Burghardt. 1983. Total internal reflection fluorescent microscopy. *J. Microscopy.* 129:19–28.
6. Beckerle, M. C., D. E. Miller, M. E. Bertagnolli, and S. J. Locke. 1989. Activation-dependent redistribution of the adhesion plaque protein, talin, in intact human platelets. *J. Cell Biol.* 109:3333–3346.
7. Bell, G. I. 1978. Models for the specific adhesion of cells to cells. *Science (Wash. DC).* 200:618–627.
8. Bell, G. I., M. Dembo, and P. Bongrand. 1984. Cell adhesion: Competition between nonspecific repulsion and specific bonding. *Biophys. J.* 45:1051–1064.
9. Ben-Ze'ev, A., S. R. Farmer, and S. Penman. 1980. Protein synthesis requires cell-surface contact while nuclear events respond to cell shape in anchorage-dependent fibroblasts. *Cell.* 21:365–372.
10. Ben-Ze'ev, A., G. S. Robinson, N. L. Bucher, and S. R. Farmer. 1988. Cell-cell and cell-matrix interactions differentially regulate the expression of hepatic and cytoskeletal genes in primary cultures of rat hepatocytes. *Proc. Natl. Acad. Sci. USA.* 85:2161–2165.
11. Buck, C. A., and A. F. Horwitz. 1987. Cell surface receptors for extracellular matrix molecules. *Annu. Rev. Cell Biol.* 3:179–205.
12. Burridge, K., and L. Connell. 1983. Talin: A cytoskeletal component concentrated in adhesion plaques and other sites of actin-membrane interaction. *Cell Motil.* 3:405–417.
13. Burridge, K., K. Fath, T. Kelly, G. Nuckolls, and C. Turner. 1988. Focal adhesions: transmembrane junctions between the extracellular matrix and the cytoskeleton. *Annu. Rev. Cell Biol.* 4:487–525.
14. Burridge, K., and P. Mangeat. 1984. An interaction between vinculin and talin. *Nature (Lond.).* 308:744–746.
15. Chen, W.-T., J. Wang, T. Hasegawa, S. S. Yamada, and K. M. Yamada. 1986. Regulation of fibronectin receptor distribution

by transformation, exogenous fibronectin, and synthetic peptides. *J. Cell Biol.* 103:1649–1661.

16. Couchman, J. R., and D. A. Rees. 1979. The behaviour of fibroblasts migrating from chick heart explants: changes in adhesion, locomotion and growth, and in the distribution of actomyosin and fibronectin. *J. Cell Sci.* 39:149–165.
17. Cozens-Roberts, C., J. A. Quinn, and D. A. Lauffenburger. 1990. Receptor-mediated adhesion phenomena. Model studies with the radial-flow detachment assay. *Biophys. J.* 58:107–125.
18. Danilov, Y. N., and R. L. Juliano. 1989. $(Arg\text{-}Gly\text{-}Asp)_n$-albumin conjugates as a model substratum for integrin-mediated cell adhesion. *Exp. Cell Res.* 182:186–196.
19. Dejana, E., S. Colella, G. Conforti, M. Abbadini, M. Gaboli, and P. C. Marchisio. 1988. Fibronectin and vitronectin regulate the organization of their respective Arg-Gly-Asp adhesion receptors in cultured human endothelial cells. *J. Cell Biol.* 107:1215–1223.
20. Dembo, M., and F. Harlow. 1986. Cell motion, contractile networks, and the physics of interpenetrating reactive flow. *Biophys. J.* 50:109–121.
21. Dembo, M., D. C. Torney, K. Saxman, and D. Hammer. 1988. The reaction-limited kinetics of membrane-to-surface adhesion and detachment. *Proc. R. Soc. Lond. B.* 234:55–83.
22. DePasquale, J. A., and C. S. Izzard. 1991. Accumulation of talin in nodes at the edge of the lamellipodium and separate incorporation into adhesion plaques at focal contacts in fibroblasts. *J. Cell Biol.* 113(6):1351–1359.
23. DiMilla, P. A., K. Barbee, and D. A. Lauffenburger. 1991. Mathematical model for the effects of adhesion and mechanics on cell migration speed. *Biophys. J.* 60:15–37.
24. Duband, J.-L., G. H. Nuckolls, A. Ishihara, T. Hasegawa, K. M. Yamada, J. P. Thiery, and K. Jacobson. 1988. Fibronectin receptor exhibits high lateral mobility in embryonic locomoting cells but is immobile in focal contacts and fibrillar streaks in stationary cells. *J. Cell Biol.* 107:1385–1396.
25. Dustin, M. L., and T. A. Springer. 1989. T-cell receptor cross-linking transiently stimulates adhesiveness through LFA-1. *Nature (Lond.).* 341:619–624.
26. Duwe, H. P., J. Kaes, and E. Sackmann. 1990. Bending elastic moduli of lipid bilayers: modulation by solutes. *J. Phys. France.* 51:945–962.
27. Engelhardt, H., H. P. Duwe, and E. Sackmann. 1985. Bilayer bending elasticity measured by Fourier analysis of thermally excited surface undulations of flaccid vesicles. *J. Physique Lett.* 46:395–400.
28. Evans, E. A. 1983. Bending elastic modulus of red blood cell membrane derived from buckling instability in micropipet aspiration tests. *Biophys. J.* 43:27–30.
29. Evans, E. A. 1985*a*. Detailed mechanics of membrane-membrane adhesion and separation. I. Continuum of molecular cross-bridges. *Biophys. J.* 48:175–183.
30. Evans, E. A. 1985*b*. Detailed mechanics of membrane-membrane adhesion and separation. II. Discrete kinetically trapped molecular cross-bridges. *Biophys. J.* 48:185–192.
31. Evans, E., D. Berk, and A. Leung. 1991. Detachment of agglutinin-bonded red blood cells. I. Forces to rupture molecular-point attachments. *Biophys. J.* 59:838–848.
32. Evans, E., and D. Needham. 1986. Giant vesicle bilayers composed of mixtures of lipids, cholesterol, and polypeptides. Thermomechanical and (mutual) adherence properties. *Faraday Discussions Chem. Soc.* 81:267–280.
33. Evans, E. A., R. Waugh, and L. Melnik. 1976. Elastic area compressibility modulus of red cell membrane. *Biophys. J.* 16:585–595.
34. Fath, K. R., C.-J. Edgell, and K. Burridge. 1989. The distribution of distinct integrins in focal contacts is determined by the substratum composition. *J. Cell Sci.* 92:67–75.
35. Feltkamp, C. A., M. A. Pijnenberg, and E. Roos. 1991. Organization of talin and vinculin in adhesion plaques of wet-cleaved chicken embryo fibroblasts. *J. Cell Sci.* 100:579–587.
36. Folkman, J., and A. Moscona. 1978. Role of cell shape in growth control. *Nature (Lond.).* 273:345–349.
37. Gingell, D., I. Todd, and J. Bailey. 1985. Topography of cell-glass apposition revealed by total internal reflection fluorescence of volume markers. *J. Cell Biol.* 100:1334–1338.
38. Hammer, D. A., and D. A. Lauffenburger. 1987. A dynamical model for receptor-mediated cell adhesion to surfaces. *Biophys. J.* 52:475–487.
39. Horwitz, A., K. Duggan, C. Buck, M. C. Beckerle, and K. Burridge. 1986. Interaction of plasma membrane fibronectin receptor with talin-a transmembrane linkage. *Nature (Lond.).* 320:531–533.
40. Harris, A. 1973. Location of cellular adhesions to solid substrata. *Dev. Biol.* 35:97–114.
41. Hynes, R. O. 1990. Fibronectins. Springer-Verlag, New York. 546 pp.
42. Ingber, D. E. 1990. Fibronectin controls capillary endothelial cell growth by modulating cell shape. *Proc. Natl. Acad. Sci. USA.* 87:3579–3583.
43. Ingber, D. E., and J. Folkman. 1989. Mechanochemical switching between growth and differentiation during fibroblast growth factor-stimulated angiogenesis in vitro: role of extracellular matrix. *J. Cell Biol.* 109:317–330.
44. Izzard, C. S., and L. R. Lochner. 1976. Cell-to-substrate contacts in living fibroblasts: an interference-reflexion study with an evaluation of the technique. *J. Cell Sci.* 21:129–159.
45. Izzard, C. S., and L. R. Lochner. 1980. Formation of cell-to-substrate contacts during fibroblast motility: An interference-reflexion study. *J. Cell Sci.* 42:81–116.
46. Jones, G. E., R. G. Arumugham, and M. L. Tanzer. 1986. Fibronectin glycosylation modulates fibroblast adhesion and spreading. *J. Cell Biol.* 103:1663–1670.
47. Kolega, J., M. S. Shure, W.-T. Chen, and N. D. Young. 1982. Rapid cellular translocation is related to close contacts formed between various cultured cells and their substrata. *J. Cell Sci.* 54:23–34.
48. Kumagai, H., M. Tajima, Y. Ueno, Y. Giga-Hama, and M. Ohba. 1991. Effect of cyclic RGD peptide on cell adhesion and tumor metastasis. *Biochem. Biophys. Res. Comm.* 177:74–82.
49. Lotz, M. M., C. A. Burdsal, H. P. Erickson, and D. R. McClay. 1989. Cell adhesion to fibronectin and tenascin: quantitative measurements of initial binding and subsequent strengthening response. *J. Cell Biol.* 109:1795–1805.
50. Marcantonio, E. E., J.-L. Guan, J. E. Trevithick, and R. O. Hynes. 1990. Mapping of the functional determinants of the integrin β_1 cytoplasmic domain by site-directed mutagenesis. *Cell Regulation.* 1:597–604.
51. Massia, S. P., and J. A. Hubbell. 1990. Covalent surface immobilization of Arg-Gly-Asp- and Tyr-Ile-Gly-Ser-Arg-containing peptides to obtain well-defined cell-adhesive surfaces. *Anal. Biochem.* 187:292–301.
52. Massia, S. P., and J. A. Hubbell. 1991. An RGD spacing of 440 nm is sufficient for integrin $\alpha_v\beta_3$-mediated fibroblast spreading and 140 nm for focal contact and stress fiber formation. *J. Cell Biol.* 114(5):1089–1100.
53. Molony, L., D. McCaslin, J. Abernethy, B. Paschal, and K.

Burridge. 1987. Properties of talin from chicken gizzard smooth muscle. *J. Biol. Chem.* 262(16):7790–7795.

54. Mueller, S. C., T. Kelly, M. Dai, H. Dai, and W.-T. Chen. 1989. Dynamic cytoskeleton-integrin associations induced by cell binding to immobilized fibronectin. *J. Cell Biol.* 109:3455–3464.
55. Nuckolls, G. H., C. E. Turner, and K. Burridge. 1990. Functional studies of the domains of talin. *J. Cell Biol.* 110:1635–1644.
56. O'Neill, C., P. Jordan, and G. Ireland. 1986. Evidence for two distinct mechanisms of anchorage stimulation in freshly explanted and 3T3 Swiss mouse fibroblasts. *Cell.* 44:489–496.
57. Otey, C. A., F. M. Pavalko, and K. Burridge. 1990. An interaction between α-actinin and the β_1 integrin subunit in vitro. *J. Cell Biol.* 111:721–729.
58. Otto, J. J. 1990. Vinculin. *Cell Motil. Cytoskeleton.* 16:1–6.
59. Pecht, I., and D. Lancet. 1977. Kinetics of antibody-hapten interactions. *Mol. Biol. Biochem. Biophys.* 24:306–338.
60. Rees, D. A., C. W. Lloyd, and D. Thom. 1977. Control of grip and stick in cell adhesion through lateral relationships of membrane glycoproteins. *Nature (Lond.).* 267:124–128.
61. Reszka, A. A., Y. Hayashi, and A. F. Horwitz. 1992. Identification of amino acid sequences in the integrin β_1 cytoplasmic domain implicated in cytoskeletal association. *J. Cell Biol.* 117:1321–1330.
62. Tapley, P., A. Horwitz, C. Buck, K. Duggan, and L. Rohrschneider. 1989. Integrins isolated from Rous sarcoma virus-transformed chicken embryo fibroblasts. *Oncogene.* 4:325–333.
63. Tha, S. P., and H. L. Goldsmith. 1988. Interaction forces between red cells agglutinated by antibody. III. Micromanipulation. *Biophys. J.* 53:677–687.
64. Tözeren, A., K.-L. Sung, and S. Chien. 1989. Theoretical and experimental studies on cross-bridge migration during cell disaggregation. *Biophys. J.* 55:479–487.
65. Tözeren, A., K.-L. Sung, L. A. Sung, M. L. Dustin, P.-Y. Chan, T. A. Springer, and S. Chien. 1992. Micromanipulation of adhesion of a Jurkat cell to a planar bilayer membrane containing lymphocyte function-associated antigen 3 molecules. *J. Cell Biol.* 116(4):997–1006.
66. Watt, F. M., P. W. Jordan, and C. H. O'Neill. 1988. Cell shape controls terminal differentiation of human epidermal keratinocytes. *Proc. Natl. Acad. Sci. USA.* 85:5576–5580.
67. Wayner, E. A., R. A. Orlando, and D. A. Cheresh. 1991. Integrins $\alpha_v\beta_3$ and $\alpha_v\beta_5$ contribute to cell attachment to vitronectin but differentially distribute on the cell surface. *J. Cell Biol.* 113(4):919–929.
68. Weiss, L. 1961. Studies on cellular adhesion in tissue culture. IV. The alteration of substrata by cell surfaces. *Exp. Cell Res.* 25:504–517.
69. Weiss, L., and P. J. Lachmann. 1964. The origin of an antigenic zone surrounding HeLa cells cultured on glass. *Exp. Cell Res.* 36:86–91.